

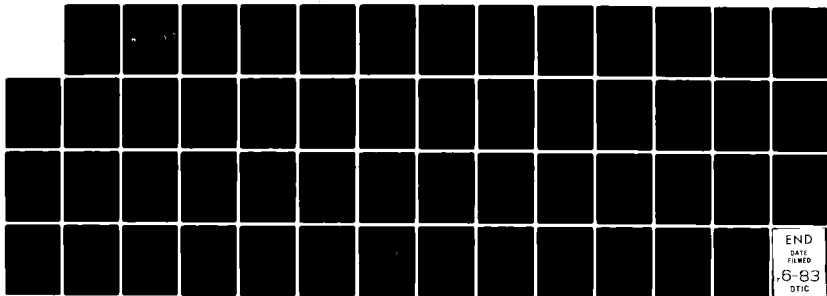
AD-A128 759 THERMONUCLEAR BURN IN CYLINDRICAL TARGETS(U) MISSION
RESEARCH CORP ALBUQUERQUE NM J BUFF ET AL. MAY 83
AFWL-TR-82-152 F29601-82-C-0040

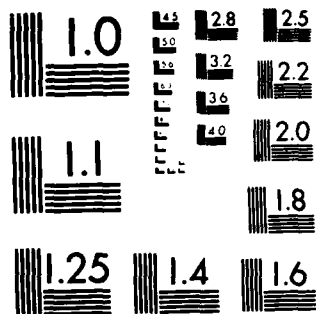
1/1

UNCLASSIFIED

F/G 20/8

NL





MICROCOPY RESOLUTION TEST CHART
NATIONAL BUREAU OF STANDARDS-1963-A

THERMONUCLEAR BURN IN CYLINDRICAL TARGETS

J. Buff
M. Alme

Mission Research Corporation
1720 Randolph Rd S.E.
Albuquerque, NM 87106

May 1983

Final Report

Approved for public release; distribution unlimited.

AIR FORCE WEAPONS LABORATORY
Air Force Systems Command
Kirtland Air Force Base, NM 87117

DTIC
ELECTE
JUN 1 1983
H

AD A128759

DTIC FILE COPY



83 05 31 140

This final report was prepared by the Mission Research Corporation, Albuquerque, New Mexico, under Contract F29601-82-C-0040, Job Order 88091717 with the Air Force Weapons Laboratory, Kirtland Air Force Base, New Mexico. Capt James A. Lupo (NTYP) was the Laboratory Project Officer-in-Charge.

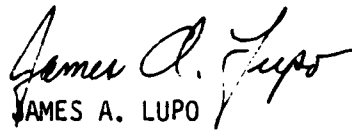
When Government drawings, specifications, or other data are used for any purpose other than in connection with a definitely Government-related procurement, the United States Government incurs no responsibility or any obligation whatsoever. The fact that the Government may have formulated or in any way supplied the said drawings, specifications, or other data, is not to be regarded by implication, or otherwise in any manner construed, as licensing the holder, or any other person or corporation; or as conveying any rights or permission to manufacture, use, or sell any patented invention that may in any way be related thereto.


This report has been authored by a contractor of the United States Government. Accordingly, the United States Government retains a nonexclusive, royalty-free license to publish or reproduce the material contained herein, or allow others to do so, for the United States Government purposes.

This report has been reviewed by the Public Affairs Office and is releasable to the National Technical Information Services (NTIS). At NTIS, it will be available to the general public, including foreign nations.

If your address has changed, if you wish to be removed from our mailing list, or if your organization no longer employs the addressee, please notify AFWL/NTYP, Kirtland AFB, NM 87117 to help us maintain a current mailing list.

This technical report has been reviewed and is approved for publication.


JAMES A. LUPO
Capt, USAF
Project Officer


JOHN I. GENEROSA
Lt Col, USAF
Chief, Simulators & Adv Wpns Br

FOR THE COMMANDER

ALAN R. COLE
Colonel, USAF
Chief, Advanced Technology Division

DO NOT RETURN COPIES OF THIS REPORT UNLESS CONTRACTUAL OBLIGATIONS OR NOTICE ON A SPECIFIC DOCUMENT REQUIRES THAT IT BE RETURNED.

UNCLASSIFIED

SECURITY CLASSIFICATION OF THIS PAGE (When Data Entered)

REPORT DOCUMENTATION PAGE		READ INSTRUCTIONS BEFORE COMPLETING FORM
1. REPORT NUMBER AFWL-TR-82-152	2. GOVT ACCESSION NO. AD-A128	3. RECIPIENT'S CATALOG NUMBER 759
4. TITLE (and Subtitle) THERMONUCLEAR BURN IN CYLINDRICAL TARGETS		5. TYPE OF REPORT & PERIOD COVERED Final Report
7. AUTHOR(s) J. Buff M. Alme		6. PERFORMING ORG. REPORT NUMBER
9. PERFORMING ORGANIZATION NAME AND ADDRESS Mission Research Corporation 1720 Randolph Rd, SE Albuquerque, NM 87106		8. CONTRACT OR GRANT NUMBER(s) F29601-82-C-0040
11. CONTROLLING OFFICE NAME AND ADDRESS Air Force Weapons Laboratory (NTYP) Kirtland Air Force Base, NM 87117		10. PROGRAM ELEMENT, PROJECT, TASK AREA & WORK UNIT NUMBERS 62601F/88091717
14. MONITORING AGENCY NAME & ADDRESS (if different from Controlling Office)		12. REPORT DATE May 1983
		13. NUMBER OF PAGES 50
		15. SECURITY CLASS. (of this report) Unclassified
		15a. DECLASSIFICATION/DOWNGRADING SCHEDULE
16. DISTRIBUTION STATEMENT (of this Report) Approved for public release; distribution unlimited.		
17. DISTRIBUTION STATEMENT (of the abstract entered in Block 20, if different from Report)		
18. SUPPLEMENTARY NOTES		
19. KEY WORDS (Continue on reverse side if necessary and identify by block number) Inertial Fusion Magnetic Fields Imploding Plasmas Thermonuclear <i>10 to the 15th power</i> <i>10 to the 18th power</i>		
20. ABSTRACT (Continue on reverse side if necessary and identify by block number) Thermonuclear burn in cylindrical targets imploded by fast plasma linear devices are considered. The benefits of limiting the thermal conduction and trapping the alpha particles as might be expected in the presence of a strong magnetic field are studies. It will be extremely difficult to achieve good thermonuclear burn in cylindrical targets with fast plasma liner devices. However, a large neutron flux (10^{15} - 3×10^{16}) can be achieved, which may be a powerful diagnostic in determining the quality of the plasma implosion.		

DD FORM 1 JAN 73 1473

EDITION OF 1 NOV 65 IS OBSOLETE

UNCLASSIFIED

SECURITY CLASSIFICATION OF THIS PAGE (When Data Entered)

UNCLASSIFIED

SECURITY CLASSIFICATION OF THIS PAGE(When Data Entered)

Accession For	
NTIS GRA&I	<input checked="checked" type="checkbox"/>
DTIC TAB	<input type="checkbox"/>
Unannounced	<input type="checkbox"/>
Justification	
By _____	
Distribution/	
Availability Codes	
Dist	Avail and/or Special
A	



UNCLASSIFIED

SECURITY CLASSIFICATION OF THIS PAGE(When Data Entered)

CONTENTS

<u>Section</u>		<u>Page</u>
I	INTRODUCTION	5
II	COMPRESSION REQUIREMENTS	8
III	MAGNETIC FIELDS TO INHIBIT THERMAL CONDUCTION AND TRAP ALPHA PARTICLES	9
IV	TAMPED CYLINDRICAL TARGETS	12
	1. Description of Calculations	12
	2. Results	13
	a. $\rho_f R_f = 0.1 \text{ g/cm}^2$	16
	b. $\rho_f R_f = 0.01 \text{ g/cm}^2$	16
	c. Thermal Conductivity	17
	3. Conclusions and Discussion	19
V	LOW COMPRESSION TARGETS	21
VI	NEUTRON PRODUCTION	23
	1. Introduction and Motivation	23
	2. Description of Calculations and Selection of Parameters	24
	3. Results	27
VII	FINAL COMMENTS	47
	REFERENCES	48

ILLUSTRATIONS

<u>Figure</u>		<u>Page</u>
1	Schematic of the initial density distribution.	13
2	Fraction of DT fuel burned versus tamper mass for $\rho_f R_f = 0.1 \text{ g/cm}^2$.	14
3	Fraction of DT fuel burned versus tamper mass for $\rho_f R_f = 0.01 \text{ g/cm}^2$.	15
4	Fraction of DT fuel burned versus tamper density.	18
5	Temperature, energy flux, velocity, and density at time $t = 0$ for Models 6 and 2.	28
6	Temperature, energy flux velocity, and density at time $t = 4 \text{ ns}$ for Model 6.	29
7	Temperature, energy flux, velocity, and density at time $t = 8 \text{ ns}$ for Model 6.	30
8	Temperature, energy flux, velocity, and density at time $t = 12 \text{ ns}$ for Model 6.	31
9	Temperature, energy flux, velocity, and density at time $t = 14 \text{ ns}$ for Model 6.	32
10	Temperature, energy flux, velocity, and density at time $t = 16 \text{ ns}$ for Model 6.	33
11	Temperature, energy flux, velocity, and density at time $t = 18 \text{ ns}$ for Model 6.	34
12	Ion temperature, density, pressure, velocity, yield rate, and energy histories for Model 6.	36
13	Temperature, energy flux, velocity, and density at time $t = 4 \text{ ns}$ for Model 2.	38
14	Temperature, energy flux, velocity, and density at time $t = 8 \text{ ns}$ for Model 2.	39
15	Temperature, energy flux, velocity, and density at time $t = 12 \text{ ns}$ for Model 2.	40

ILLUSTRATIONS (Concluded)

<u>Figure</u>		<u>Page</u>
16	Temperature, energy flux, velocity, and density at time $t = 16$ ns for Model 2.	41
17	Temperature, energy flux, velocity, and density at time $t = 20$ ns for Model 2.	42
18	Temperature, energy flux, velocity, and density at time $t = 28$ ns for Model 2.	43
19	Ion temperature, density, pressure, velocity, yield rate, and energy histories for Model 2.	44

TABLES

<u>Table</u>		<u>Page</u>
1	Neutron Production	26

I. INTRODUCTION

The direct coupling approach to inertial fusion, in which an imploding cylindrical foil liner impacts a cylindrical target placed inside the foil, is unique among the current approaches in that the target driving energy is already in the form of inward directed kinetic energy. Since a goal of fusion target design is to convert energy of a given initial form into directed kinetic energy of the pusher and fuel, the fact that the liner energy is already in inward kinetic energy may be extremely helpful. No intermediate energy conversion steps are necessary. For example, in fusion with CO₂ lasers, the laser energy is converted into the energy of hot electrons at the critical surface. These electrons then heat the ablator. Material in the ablator is driven off at high velocities, which results in inward kinetic energy for the pusher and fuel. In this process, only a small fraction of the laser energy is ultimately converted into kinetic energy in the pusher and fuel. Concepts which use X-ray radiation to drive targets also require some intermediate energy conversion steps. On the other hand, the cylindrical symmetry inherent in imploding liner systems, means that cylindrical targets must probably be used in the direct coupling approach. (Concepts in which the imploding liner is coupled to a spherical target have been suggested, but their feasibility has yet to be demonstrated (Refs. 1 through 3).) This presents a problem since it is more difficult to obtain high compression in a cylindrical target than in a spherical target.

The concept of imploding a cylindrical deuterium-tritium (DT) target with an imploding liner has received considerable attention during the past decade. However, previous work has focused on the compression and heating of low density DT gas by a relatively slow liner (Refs. 4 through 12). In general, the results have been disappointing in that very high input energies were required to achieve only modest energy gains. Current or planned pulsed power experiments promise higher energies with shorter implosion timescales. Therefore, it is desirable to perform a study with input parameters appropriate to this new generation of pulsed power machines.

The SHIVA experiment at the Air Force Weapons Laboratory (AFWL) is of particular interest for this concept. The SHIVA STAR experiment, which is currently being made operational, has a 6-MJ fast capacitor bank which is used with inductive storage--opening switch pulse sharpening to drive 300 to 500 ns, 30 to 50 cm/ μ s, 400 kJ to 1 MJ, plasma shells having axial length on the order of 2 cm. Previous experiments at AFWL have used a 1.9 MJ capacitor bank to implode plasmas with kinetic energy 200 to 250 kJ (Ref. 13).

Thermonuclear burn in spherical targets has been the subject of intense study during the past 10 years. Consideration of the Lawson criterion and numerous numerical studies have shown that bare DT spheres must be compressed so that $\int \rho dR \gtrsim 0.3 - 1.0 \text{ g/cm}^2$ and temperature $T \gtrsim 3\text{-}10 \text{ keV}$ in order to obtain good thermonuclear burn. In addition, Mason and Morse (Ref. 14) have shown that a fixed amount of fuel gives an increased yield for a given $\rho_f R_f$ and ignites at a lower $\rho_f R_f$ if tamping is added, where ρ_f and R_f are the fuel density and radius.

Obtaining $\rho_f R_f \gtrsim 0.3 \text{ g/cm}^2$ is likely to be extremely difficult in cylindrical systems, as shown in Section II. Hence, it is important to determine if significant thermonuclear burn can occur in tamped cylindrical targets which have $\rho_f R_f < 0.3 \text{ g/cm}^2$. Also, an axial magnetic field can be injected into a cylindrical system. This field could thermally insulate the DT fuel from the tamper and could also help to confine the alpha particles emitted by the DT reactions. Thus, some fraction of the liberated energy could be kept in the fuel instead of being lost to the tamper.

In Section II, the difficulty of achieving high compression in cylindrical targets is illustrated. In Section III, estimates of the magnetic field strength required to trap the alpha particles emitted during the DT reaction and to inhibit the electron and ion thermal conduction are made.

In Section IV, calculations of thermonuclear burn in tamped targets are presented. The effects of suppressing the thermal conductivity and trapping the alpha particles are considered. In Section V, low compression targets are considered and the conclusion is reached that these targets are not appropriate for fast liner systems such as the SHIVA system. In Section VI, models for the production of large fluxes of neutrons with the SHIVA STAR experiment are considered.

The major conclusion from this study is that cylindrical targets are not suitable targets for fast liner experiments like the SHIVA STAR. The compression requirements for the fuel are too severe, given the symmetry of fast imploding plasma devices. However, large quantities of neutrons (10^{15} to 3×10^{16}) may be produced in the SHIVA system. This could be extremely useful for diagnostic purposes.

II. COMPRESSION REQUIREMENTS

The purpose of this section is to illustrate the difficulty in obtaining high compression in cylindrical targets as opposed to the relative ease in spherical targets. As mentioned in the Introduction, the Lawson criterion and numerous numerical studies show that $\int \rho dr \approx 0.3$ to 1.0 g/cm^2 for good thermonuclear burn in untamped targets. Clearly, it is easier to obtain higher $\int \rho dr$ in targets with larger fuel mass. However, the energy requirements are such that only a fraction of a milligram of DT can be brought to burn temperature.

For a constant density sphere of mass m_s , density ρ_s , and radius R_s ,

$$\rho_s R_s = \frac{3m_s}{4\pi R_s^2} \quad (1)$$

For a corresponding cylinder of length L ,

$$\rho_l R_l = \frac{M_l}{\pi L R_l} \quad (2)$$

In a sphere $\rho R \propto 1/R_s^2$, but in a cylinder $\rho R \propto 1/R_l$. Consider an example where $\rho R = 1 \text{ g/cm}^2$ and $m = 0.1 \text{ mg}$. For a constant density sphere, Equation 1 gives a density of 205 g/cm^2 , which is a factor 10^3 higher density than solid DT. For a corresponding cylinder with $L = 1 \text{ cm}$, Equation 2 gives a density of $3.14 \times 10^4 \text{ g/cm}^3$, which is a factor of more than 10^5 higher density than solid DT. In spherical systems it is experimentally difficult to achieve compressions of 10^3 over solid density; compressions of a factor 10^5 are clearly impossible given the symmetry of current available in imploding linear systems.

Thus, systems in which massive tampers hold the DT fuel together are studied. In such systems, only volume ignition of the fuel is possible; it is not realistic to expect hot spot ignition and propagating burn as will be shown in the next section.

III. MAGNETIC FIELDS TO INHIBIT THERMAL CONDUCTION AND TRAP ALPHA PARTICLES

The idea that magnetic fields can be used to inhibit thermal conduction and trap the alpha particles emitted during the DT reactions is not new. This idea has been examined by numerous researchers (Ref. 15) over the years. This section presents simple estimates of the magnetic field strength required to be effective.

Stronger magnetic fields are required to inhibit the ion thermal conduction than to inhibit the electron thermal conduction. Also, in some cases of interest, the electron and ion temperatures will not be equal. It is of interest to examine ion and electron conduction separately.

The magnetic field can inhibit thermal conduction in a direction perpendicular to the magnetic field when $\omega_e \tau_e \gg 1$, where ω_e is the electron cyclotron frequency given by

$$\omega_e (\mu s^{-1}) = 1.76 \times 10^7 B(MG) \quad (3)$$

and τ_e is the electron self-collision time given by

$$\tau_e (\mu s) = 1.835 \times 10^{-8} \frac{A}{Z} \frac{T_e^{3/2}}{\rho \ln \Lambda} \quad (4)$$

T_e is the electron temperature in keV, ρ is the density in g/cm³, A is the atomic weight, Z is the atomic number, and $\ln \Lambda$ is the coulomb logarithm (Refs. 16, 17). Furthermore, the electron thermal conductivity will be reduced over the classical value (without magnetic fields) by a factor of approximately $F_e = (\omega_e \tau_e)^2$ if $\omega_e \tau_e \gg 1$. So

$$F_e = 0.104 \frac{B^2(MG) T_e^3}{\rho^2} \left(\frac{A}{Z} \right)^2 \frac{1}{(\ln \Lambda)^2} \quad (5)$$

There is a strong dependence on B , T , and ρ . Thus, the thermal conductivity can more easily be suppressed in a low density, low compression target

than in a high density, high compression target. For $A/Z = 2.5$ appropriate for DT and $ln\Lambda = 5$, Equation 5 becomes

$$F_e = 2.5 \times 10^3 \left(\frac{B}{10 \text{ MG}} \right)^2 \left(\frac{T}{10 \text{ keV}} \right)^3 \rho^{-2} \quad (6)$$

which shows that the electron thermal conduction can be reduced by a huge factor in imploding liner devices.

The ion thermal conductivity is inhibited by the magnetic field when $\omega_i \tau_i \gg 1$, where ω_i is the ion cyclotron frequency given by

$$\omega_i (\mu s^{-1}) = 9.6 \times 10^3 \left(\frac{Z}{A} \right) B(\text{MG}) \quad (7)$$

and τ_i is the ion self collision time given by

$$\tau_i (\mu s) = 1.113 \times 10^{-6} \frac{A^{3/2} T_i^{3/2}}{Z^4 \rho ln\Lambda} \quad (8)$$

Defining $F_i = (\omega_i \tau_i)^2$,

$$F_i = 1.4 \times 10^{-4} \frac{B^2(\text{MG}) T_i^3}{\rho^2} \frac{A}{Z^6 (ln\Lambda)^2}$$

or

$$F_i = \left(\frac{B}{10 \text{ MG}} \right)^2 \left(\frac{T_i}{10 \text{ keV}} \right)^3 \rho^{-2} \quad (9)$$

where $Z = 1$, $A = 2.5$, and $ln\Lambda = 5$. Equation 9 shows that the ion thermal conduction can also be inhibited in imploding liner devices if the density is not too high. However, stronger magnetic fields are required to inhibit the ion conduction than to inhibit the electron conduction for equal ion and electron temperatures.

For $\omega\tau \gg 1$, the thermal conductivity is reduced by a factor of approximately $(\omega\tau)^2$ over the value with no magnetic field. However, Lindemuth and Widner (Ref. 18) point out that when $\omega\tau \approx 1$, a degree of magnetothermoinsulation can be provided. A $\omega_e \tau_e$ of unity leads to a reduction factor of nearly 4.

In unmagnetized fuel, the ratio of the alpha particle range λ to the fuel radius R_f is given by approximately

$$\frac{\lambda}{R_f} = 0.06 \left(\frac{T_e}{3 \text{ keV}} \right)^{3/2} \frac{1}{\rho R_f} \quad (10)$$

Thus, in a high compression, untamped target, the confinement time requirement (Lawson criterion) of $\rho R_f > 0.3$ to 1.0 g/cm^2 is usually more severe than the alpha trapping requirements.

For the magnetic field to aid in trapping the 3.5 MeV alpha particles, the gyroradius of the alpha particle R_α must usually be smaller than the fuel radius. (One could imagine situations where this is not the case. For example, the fuel region could be surrounded by a magnetic field. As long as the alpha particles did not reach the wall or tamper, but only remained in the vacuum region or in the fuel, the alphas would eventually deposit their kinetic energy in the fuel region.) The radius of gyration for a 3.5 MeV alpha particle is given by

$$R_\alpha \text{ (cm)} = \frac{0.27}{B(\text{MG})} \quad (11)$$

Thus, it will be extremely difficult to trap the alpha particles in a high compression (small fuel radius) target by means of a magnetic field. In a low compression target where the fuel is held together by a tamper or wall, the magnetic field can be of considerable benefit.

IV. TAMPED CYLINDRICAL TARGETS

It was shown in Section II, that obtaining compressions in cylindrical targets so that $\int \rho R \approx 0.3$ to 1.0 g/cm^2 will be extremely difficult. The degree to which a tamper can reduce the compression requirements is investigated in this section along with the effects of reducing the thermal conductivity and trapping of the alpha particles as might be expected in the presence of a sufficiently strong magnetic field.

1. DESCRIPTION OF CALCULATIONS

The computations were performed with the one-dimensional (1-D) magneto-hydrodynamic radiation code MACH1 (Ref. 19 and 20). The initial conditions for the fuel and tamper were chosen as follows. The central fuel region was a cylinder of DT at initial density ρ_f and initial temperature T_f . This was surrounded by a nickel shell (the tamper) at initial density ρ_t and initial temperature T_t . As the fuel will have been compressed by the tamper, which also serves as a pusher, the pressure in the tamper is required to be equal to that in the fuel. For all the computations reported here, the fuel mass per unit length was chosen to be 0.1 mg/cm . This fuel mass is appropriate for a SHIVA-like device because it takes 58 kJ of energy to heat 0.1 mg of DT to 5 keV . It is convenient to use the variable $\rho_f R_f$ as an independent variable since the burn fraction is expected to be a strong function of $\rho_f R_f$. If the mass per unit length is fixed, $\rho_f R_f$ determines ρ_f and R_f . For most of the calculations reported here ρ_t is assumed to equal $4 \rho_f$, although at the end of Section III, the effects of varying ρ_t are discussed. Choosing a value of T_f , then gives T_t if ρ_t is known. Hence, the input parameters are $\rho_f R_f$, tamper mass/length m_t , T_f , and ρ_t . Figure 1 is a schematic of the initial density distribution.

Radiative losses were not included for the calculations reported here. The MACH1 code runs much faster if radiation is not included. In limited

Tamped Cylindrical Targets

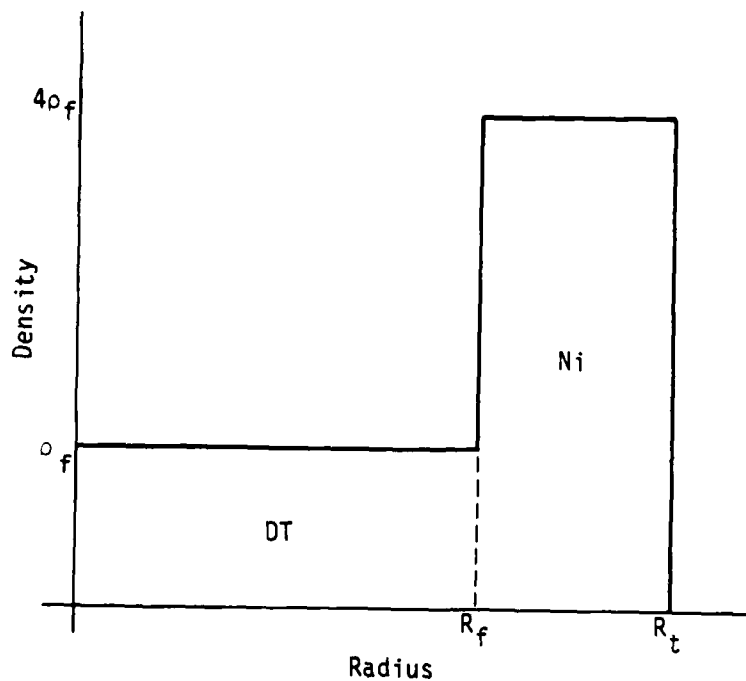


Figure 1. Schematic of the initial density distribution used in calculations.

tests, it was found that radiative losses were not important for the parameter range of most interest. In any case, radiative losses will only make the computed thermonuclear burn smaller. Classical thermal conductivity was either included or suppressed totally as one might expect in a strong magnetic field. The alpha particles emitted during the DT reaction were assumed to either escape the fuel or to be trapped locally as might be expected in the presence of a sufficiently strong magnetic field.

2. RESULTS

Figures 2 and 3 show the fraction of the DT fuel burned as a function of tamper mass for $\rho_f R_f = 0.1 \text{ g/cm}^2$ and $\rho_f R_f = 0.01 \text{ g/cm}^2$, respectively. For all points plotted in Figures 2 and 3, $\rho_t = 4 \rho_f$.

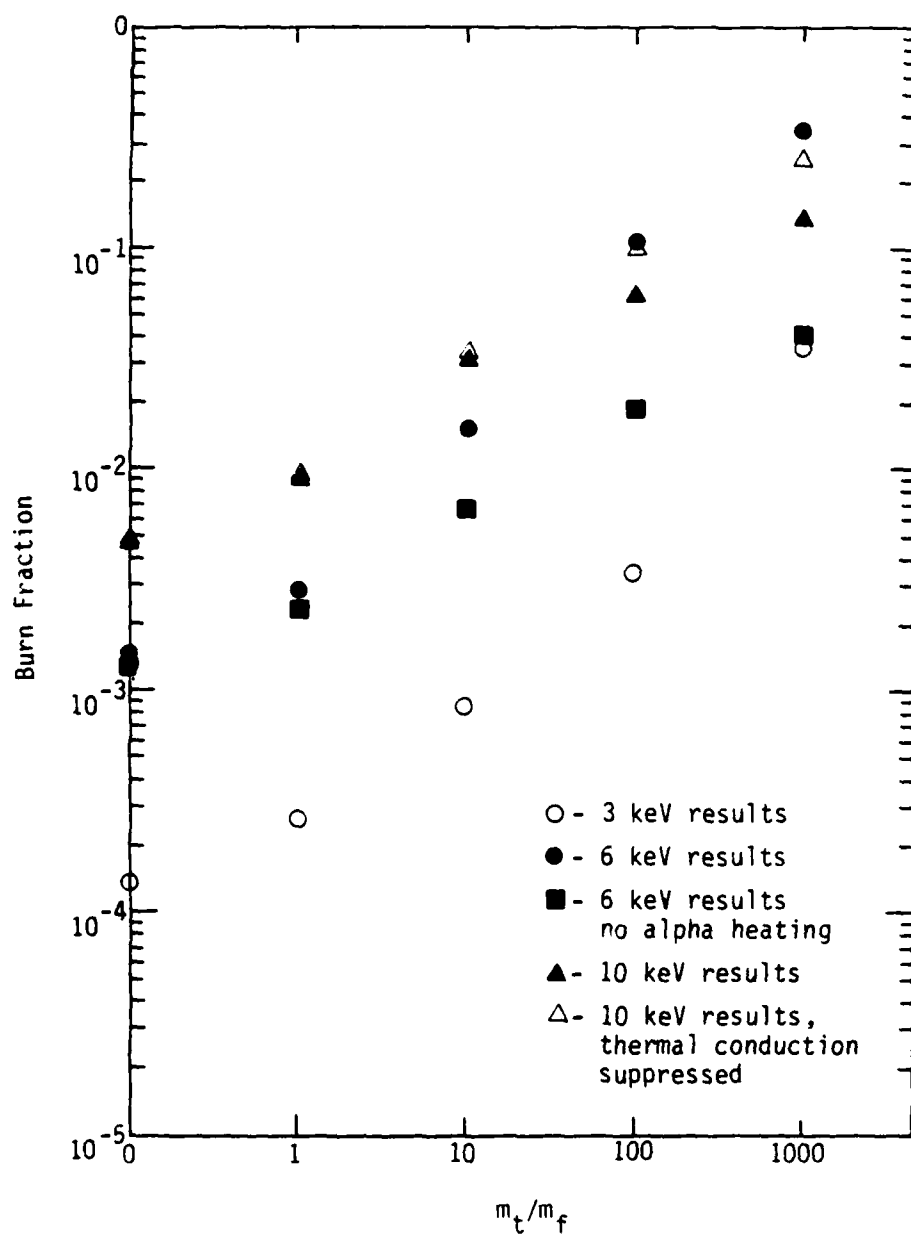


Figure 2. Fraction of DT fuel burned versus tamper mass for $\rho_f R_f = 0.1 \text{ g/cm}^2$.

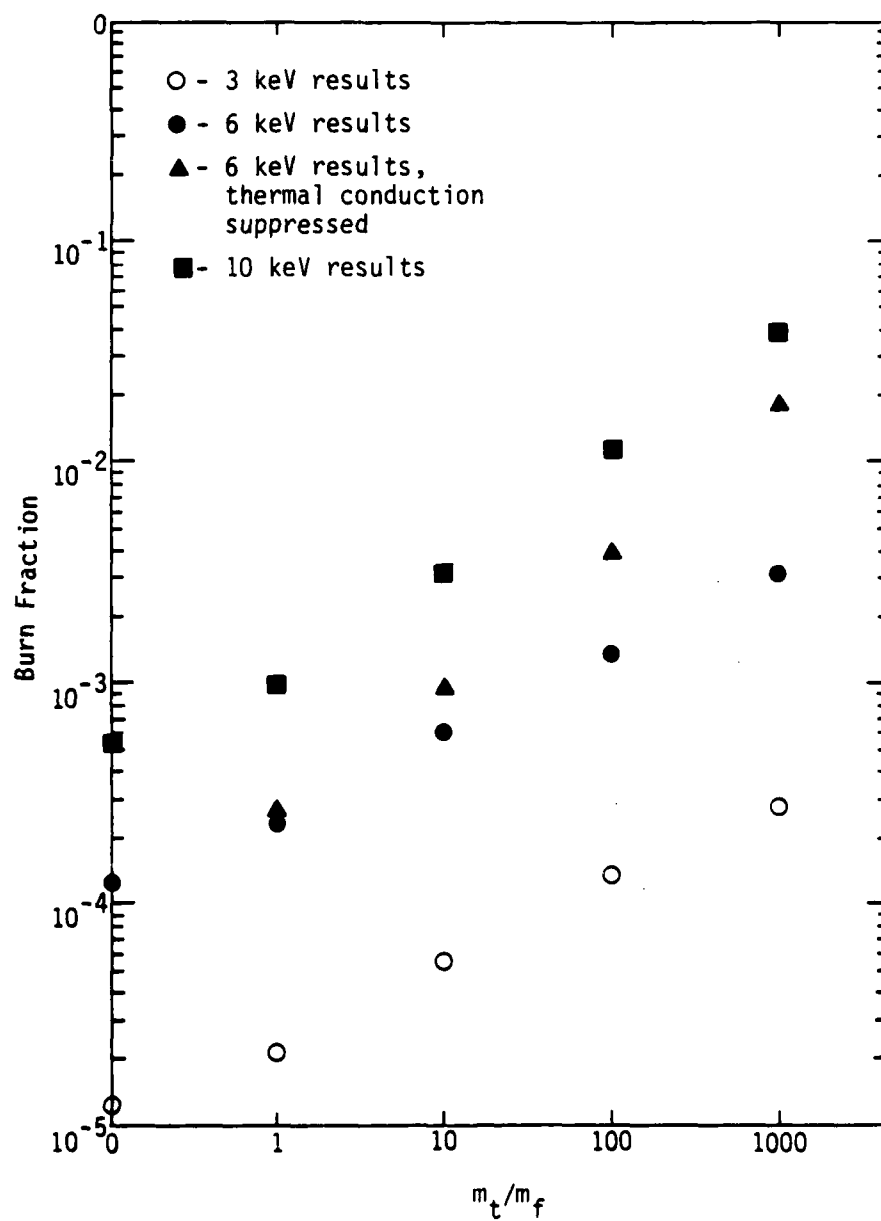


Figure 3. Fraction of DT fuel burned versus tamper mass for $\rho_f R_f = 0.01 \text{ g/cm}^2$.

a. $\rho_f R_f = 0.1 \text{ g/cm}^2$ --The open circles in Figure 2 are results for models with $T_f = 3 \text{ keV}$, local trapping of the α particles, and classical thermal conductivity. The burn fraction increases with tamper mass from 1.3×10^{-4} for a bare DT sphere to 0.035 for a tamper mass of 1000 m_f . This increase is almost solely due to the increased confinement time as the tamper mass is increased. Trapping of the alpha particles is only important in the $m_t = 1000 \text{ m}_f$ case. In models with lower tamper masses, the heating due to the alpha particles is not enough to raise the temperature significantly. A reasonable tamper mass for a SHIVA-like device is about 10^2 m_f , so $T_f = 3 \text{ keV}$ and $\rho_f R_f = 0.1 \text{ g/cm}^2$ are not sufficient for good burn.

The filled circles in Figure 2 are results for models identical to those described above except that $T_f = 6 \text{ keV}$. These cases are much more promising since tamper masses greater than 100 m_f give burn fractions in excess of 10 percent. Trapping of the alpha particles is critical, however. The filled squares are results when the alpha particle heating is suppressed. The burn fraction is only 2 percent at $m_t = 100 \text{ m}_f$.

Trapping of the alpha particles is not required if the DT fuel can be brought to a sufficiently high temperature. The filled triangles in Figure 2 are results for $T_f = 10 \text{ keV}$ and no heating by the alpha particles. The open triangles are results when the thermal conductivity is suppressed. Burn fractions approaching 10 percent are obtained for $m_t = 100 \text{ m}_f$. Higher burn fractions would be obtained for higher initial temperatures.

b. $\rho_f R_f = 0.01 \text{ g/cm}^2$ --Figure 3 shows the burn fraction as a function of tamper mass for $\rho_f R_f = 0.01 \text{ g/cm}^2$. The results are much worse than in the $\rho_f R_f = 0.1 \text{ g/cm}^2$ cases. The open circles are results for models with $T_f = 3 \text{ keV}$, local trapping of the α particles, and classical thermal conductivity. The burn fraction ranges from 1.2×10^{-5} for a bare cylinder to 2.7×10^{-4} for a tamper with 1000 m_f . These values are at

least an order of magnitude worse than the corresponding models with $\rho_f R_f = 0.1 \text{ g/cm}^2$.

The filled circles are results where $T_f = 6 \text{ keV}$ and include classical thermal conductivity. The results are an order of magnitude higher than in the 3 keV models, but still too low for good burn. In both the 3 and 6 keV models, it makes little difference whether the alpha particles are trapped or not. There is not enough burn to increase the gas temperature significantly.

Some increase in burn is gained by suppressing the thermal conductivity. This is illustrated by the triangles in Figure 3, which are results for $T_f = 6 \text{ keV}$ with suppressed thermal conductivity. The gain is not sufficient, however, to give good burn as the burn fraction is only 3.8×10^{-3} at $m_t = 100 m_f$.

The squares in Figure 3 are results for extremely optimistic conditions. In these models $T_f = 10 \text{ keV}$, the thermal conductivity is totally suppressed, and the alpha particles are assumed to be trapped. The burn fraction is only 10^{-2} at $m_f = 100 m_f$.

Hence for $\rho_f R_f < 0.01$, there appears to be no reasonable way to achieve good burn in tamped cylindrical targets.

c. Thermal Conductivity--In these previous results, it was assumed that $\rho_t = 4 \rho_f$. One might wonder if the burn fraction could be increased by using more dense tampers or more sophisticated tampers. The answer is no. Figure 4 shows the burn fraction as a function of tamper density for $\rho_f R_f = 0.01 \text{ g/cm}^2$, $T_f = 6 \text{ keV}$, and $m_t = 1000 m_f$. The burn fraction actually decreases dramatically as the tamper density increases. This decrease is due almost entirely to thermal conductivity. As the tamper density is increased, the tamper temperature is lowered to maintain

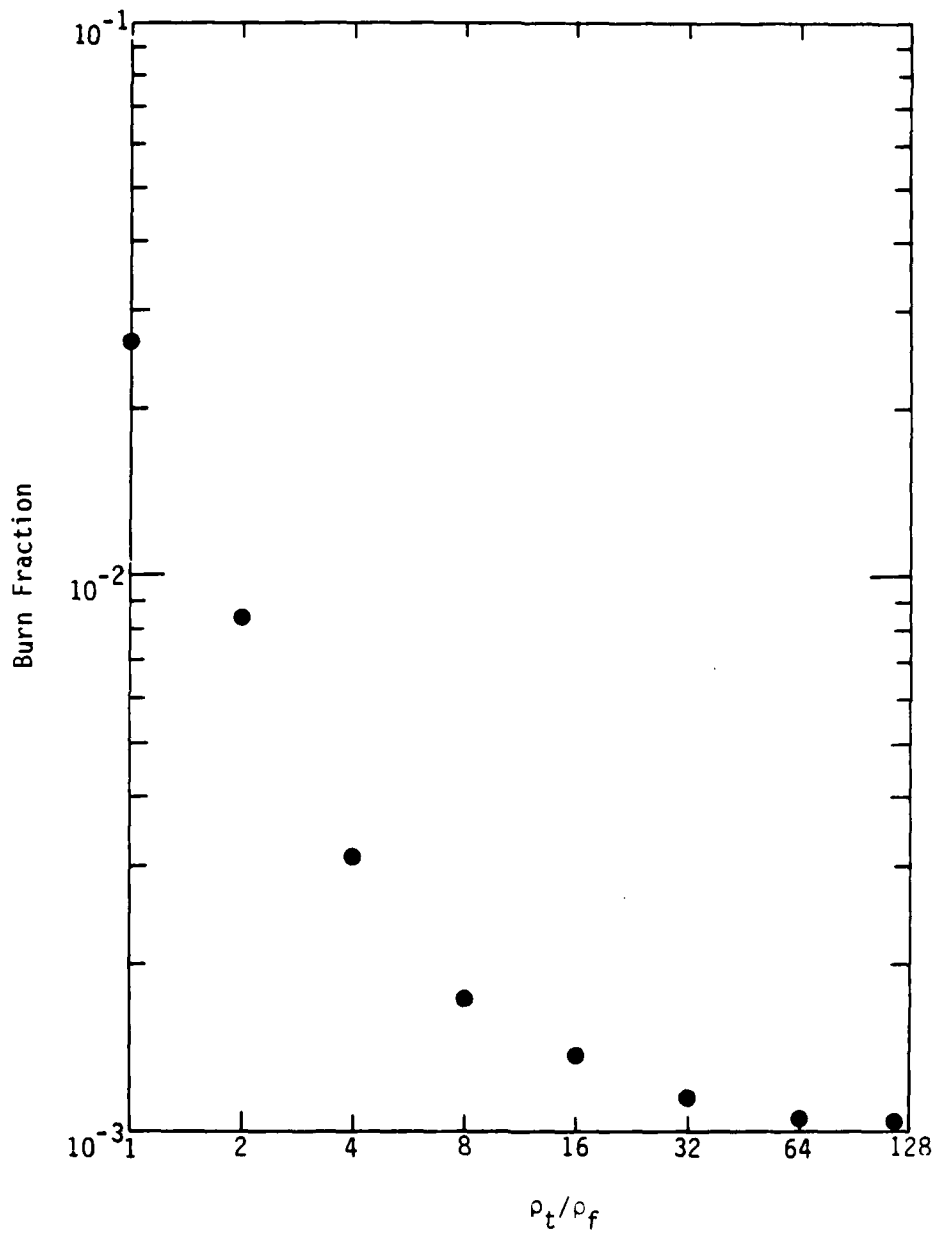


Figure 4. Fraction of DT fuel burned versus tamper density for $\rho_f R_f = 0.01 \text{ g/cm}^2$, $m_t = 1000 m_f$, and $T_f = 6 \text{ keV}$.

pressure equilibrium. The denser tampers cause excessive energy loss from the fuel to the tamper via thermal conduction. In the case where $\rho_t = \rho_f$, the tamper is hotter than the fuel and energy is actually transferred to the fuel via thermal conduction. Low density tampers are not reasonable for target designs. As the tamper density is decreased, the temperature must be increased to maintain pressure equilibrium, and the energy requirements become prohibitive. For example, the model with $\rho_t = \rho_f$ gives a burn fraction of 0.0261, but requires 76 MJ/cm in internal energy to achieve the initial configuration. Clearly, such models are not reasonable.

When thermal conduction was totally suppressed in models with $\rho R = 0.01$ g/cm², it was found that the burn fraction was almost independent of tamper density but depended strongly on tamper mass. Hence, the burn fractions shown in Figure 3 where the thermal conduction is totally suppressed are almost independent of tamper density. Since the compressed state of the tamper-pusher and fuel will be in approximate pressure equilibrium, it is likely that the use of complex tamper will not significantly increase the burn fractions above those calculated above as long as the energy requirements are reasonable. While this result has not been proven in any rigorous sense, as it is based on computer models which sample a limited range of parameter space, we feel that it is valid for the parameter range of most interest.

3. CONCLUSIONS AND DISCUSSION

The goal in this section has been to determine the conditions in the DT fuel and tamper in order to achieve significant thermonuclear burn in cylindrical systems. If the fuel can be compressed to $\rho_f R_f = 1.0$ g/cm², then good burn can be obtained if $T_f > 3$ keV. For $\rho_f R_f = 0.1$ g/cm², reasonably good burn can be obtained if the alpha particles are trapped, a tamper of 100 m_f or larger is used, and $T_f > 6$ keV.

Reasonable burn can also be obtained if $T_f > 10$ keV, even if the alpha particles are not trapped. For $\rho_f R_f = 0.01$ g/cm², significant burn could not be achieved for reasonable parameters, even with the most optimistic assumptions. These were that the alpha particles were trapped, thermal conduction was totally suppressed, and $T_f = 10$ keV.

To this point the energy requirements for the models presented have not been discussed in any detail. For massive tampers the energy requirements are critically dependent on tamper density. The energy required to raise the DT fuel is easily calculated from the temperature

$$E(\text{MJ}) = 0.115 m_f(\text{mg}) T_f(\text{keV})$$

For example, it takes 115 kJ to raise 0.1 mg of DT to 10 keV. The tamper is likely to be in pressure equilibrium with the fuel. So, the denser the tamper can be made, the less energy is required. For example, the energy required for the models discussed in connection with Figure 4 ranged from 0.42 MJ/cm to 76 MJ/cm as the tamper density decreased from 120 ρ_f to 1 ρ_f .

From the target design standpoint, the tamper must be made as dense as possible in order to reduce the energy requirements. At high tamper densities, thermal conduction must be suppressed so that the energy in the fuel is not lost to the tamper.

Reluctantly, it must be concluded that, unless targets can be compressed so that $\rho_f R_f \sim 0.1$ g/cm², then a good burn (> 10 percent) cannot be achieved in tamped cylindrical systems with reasonable parameters. For a 0.1 mg target, $\rho_f R_f = 0.1$ g/cm² requires a fuel density of 314 g/cm³, a compression of greater than 1000 over solid density. Given the symmetry in current imploding liner devices, this compression is extremely unlikely to be achieved in the near future.

V. LOW COMPRESSION TARGETS

It was shown in the previous section that it is difficult to achieve good thermonuclear burn in tamped targets unless high fuel compression can be achieved. In this section, a slightly different concept is evaluated in which the DT fuel is held together by the ram pressure of an imploding plasma liner. The model presented is very simple and crude, but it is sufficient to show the difficulties of this approach for fast liner systems such as SHIVA. More detailed models are described in References 4 and 5 and 7 through 10.

Suppose that some DT gas has been brought to thermonuclear burn temperatures (~10 keV) in some unspecified manner. It is necessary to estimate the energy required for a fast plasma liner to hold this DT gas together long enough for breakeven (so that the thermonuclear burn energy is equal to the energy required to bring the DT gas to 10 keV). It is assumed that there is sufficient magnetic field at the liner-fuel interface so that there are no thermal conduction losses.

The Lawson criterion for breakeven is

$$N\tau = 10^{14} \text{ s/cm}^3 \quad (12)$$

where N is the number density of hydrogen nuclei and τ is the confinement time. The pressure P in the DT gas is given by

$$P = 2NkT = 2 \times 10^{14} \frac{kT}{\tau} \quad (13)$$

where it has been assumed that the ion and electron temperatures T are equal. Boltzmann's constant is k . In order to confine the plasma, the ram pressure in the liner must be equal to the gas pressure in the DT fuel. Then,

$$P = \rho v^2 \approx \frac{2K}{\pi R^2} \quad (14)$$

where ρ , v , K are the liner density, velocity, and kinetic energy per unit length. R is the radius of the cylindrical liner. It has been assumed that the fuel radius is much smaller than the liner radius. Combining Equations 13 and 14,

$$K = 2 \times 10^{14} \pi R^2 kT / \tau \quad (15)$$

Making the approximation $\tau = R/v$, Equation 15 can be written as

$$K \approx 5 \text{ MJ/cm} \left(\frac{v}{10^7 \text{ cm/s}} \right) \left(\frac{R}{1 \text{ cm}} \right) \left(\frac{kT}{10 \text{ keV}} \right) \quad (16)$$

For a fast liner system such as SHIVA, $v \sim 40 \text{ cm}/\mu\text{s}$, $R \sim 1 \text{ cm}$. The energy required to confine the plasma for breakeven is clearly prohibitive for fast liner systems.

From Equation 16, K is proportional to vR . Hence, if a DT plasma is to be combined with a cylindrical liner, a slow liner which remains thin (perhaps even remains solid) is required so that the energy requirements are not enormous. This concept has been suggested by a group at Los Alamos National Laboratory (Ref. 10). Another approach would be to confine the plasma with rigid walls, supply enough magnetic field for sufficient magnetothermoinsulation, and shock heat the plasma by some other means as suggested by Kmetyk and Gross (Refs. 21 and 22).

VI. NEUTRON PRODUCTION

1. INTRODUCTION AND MOTIVATION

The previous sections have shown that good thermonuclear burn in cylindrical targets is extremely difficult with fast imploding plasma liners such as the SHIVA STAR system. This section shows that a simple system can produce large amounts of neutrons (10^{15} - 3×10^{16}) which may be useful for diagnostic purposes.

The concept put forward here is as follows. Using gas puff techniques place a small mass (about 1/100 the mass of the liner) in a column along the axis of symmetry. When the fast plasma liner impacts this low density gas, it is shock and compressionally heated to thermonuclear burn temperature. There are probably many different concepts which one could be used to produce large amounts of neutrons in an imploding liner device. Some advantages of the proposed concept are as follows. The concept and calculations based on the concept are very simple and, hence, are more reliable than a complex design. Gas puff techniques have been used in the SHIVA program before (Refs. 23 and 24). Hence, the technology already exists at AFWL to perform the experiment. Large neutron production does not require good symmetry in the imploding plasma liner. Even if hot spots are formed in the target, significant neutrons will be emitted from these hot spots. Lastly, if the emitted neutrons can be imaged, they can be a powerful diagnostic in determining the quality and symmetry of the plasma implosion. The most likely reason for the possible failure of this concept would be substantial mixing between the liner material and DT gas before thermonuclear burn conditions are achieved in the gas.

Previously, liners which have some deuterium in them have been used to produce thermonuclear neutrons at AFWL. This is not a good method if the quality of the plasma implosion is good. One-dimensional calculations show

that the neutron production in such systems is very low. In particular, one calculation was performed where a 0.5 cm thick plasma of pure DT with an energy of 350 kJ/cm and a velocity of 40 cm/ μ s was allowed to pinch on axis. The neutron production in this model was only 7×10^{12} n/cm. In this calculation, the maximum ion temperature was less than 1 keV because the internal energy was rapidly radiated away. If some amount of higher Z material had been added to the DT, the ion temperature, and hence, the neutron yield would have been much lower since the plasma would have been able to radiate much more effectively. However, in two-dimensional calculations or in experiments, the situation may be somewhat different because instabilities can cause the formation of low density regions (which may also have higher velocity) which can be shock heated and compressed by the main portion of the imploding plasma. Such a neutron production method relies on a poor quality implosion. It is more desirable to inject the low density, pure DT gas into the experiment.

2. DESCRIPTION OF CALCULATIONS AND SELECTION OF PARAMETERS

The computations were performed with the 1-D magnetohydrodynamic radiation code MACH1 (Refs. 19 and 20).

The following simple model was chosen for the computations. An outer plasma liner of uniform density, velocity, and temperature impacts a cylindrical DT target of uniform density and temperature at time $t = 0$. The computation is continued at least until the neutron production rate falls to a negligible level. Parameters appropriate to the SHIVA STAR experiment were chosen for the outer plasma sheath. A typical calculation has initial kinetic energy $E = 350$ kJ/cm, velocity $v = 40$ cm/ μ s, thickness $\Delta R_L = 0.5$ cm, and is assumed to be aluminum. For the DT fuel, a typical mass was 0.05 mg, and a typical fuel radius R_f was 0.5 cm. All of the above parameters were varied within reasonable limits. In all models the initial temperature of the plasma sheath was 5 eV, and the initial temperature of

the DT fuel was 1 eV. Input parameters for the 33 models reported on here are listed in Table 1.

Effects due to radiation were found to be important, so radiation was included in all models except two.

Thermal conductivity was also found to be extremely important. The electron thermal conduction is especially important at the fuel-liner interface. As shown in Section II, the electron thermal conductivity will be inhibited due to strong magnetic fields. It is difficult to reliably compute the magnetic field strength near this interface. The theta component of the magnetic field B_θ depends on the current flowing interior to the interface which will be difficult to compute during the pinch phase of the implosion. Even if the B_θ field is not strong enough to sufficiently impede the electron conductivity, a small B_z field (<10 kG) injected prior to the start of the liner implosion can provide the required magnetothermoinsulation at the interface. In the calculations presented here, the electron thermal conductivity is either totally suppressed or it is allowed to flow as if there were no magnetic field. In Table 1, the column labeled t.c. shows if electron thermal conductivity is allowed.

The ion thermal conductivity is not so important at the fuel-liner interface. The conductivity coefficient is usually small in the liner material because of the $1/Z^4$ dependence (see Eq. 8). Ion conduction is important at the center of the fuel region. Without ion conduction a central hot spot forms in the innermost zone. However, it will be difficult to inhibit the ion conduction at the center of the fuel region. By symmetry the B_θ field vanishes at the center, and, hopefully, a strong B_z field will not have diffused to the center of the fuel or it will impede the fuel compression. For these reasons, the ion conduction is not inhibited in the calculations presented in this report.

TABLE 1. NEUTRON PRODUCTION

Model No.	E (kJ/cm)	V cm/ μ s	Fuel mass mg	R _f cm	ΔR_L cm	t.c.	RAD	Material	Yield (10^{15} /cm.)
1	350	40	0.1	1/2	1/2	N*	Y*	Al	2.1
2	350	40	0.05	1/2	1/2	N	Y	Al	2.6
3	350	40	0.02	1/2	1/2	N	Y	Al	2.1
4	350	40	0.01	1/2	1/2	N	Y	Al	1.3
5	350	40	0.1	1/2	1/2	Y	Y	Al	0.036
6	350	40	0.05	1/2	1/2	Y	Y	Al	0.089
7	350	40	0.02	1/2	1/2	Y	Y	Al	0.60
8	350	40	0.01	1/2	1/2	Y	Y	Al	1.1
9	350	40	0.005	1/2	1/2	Y	Y	Al	0.87
10	350	40	0.05	1/2	1/2	N	Y	Ni	4.0
11	350	40	0.05	1/2	1/2	N	Y	CH	1.6
12	350	40	0.05	1/2	1/2	N	Y	Be	2.2
13	350	40	0.05	1/2	1/2	Y	Y	Ni	0.051
14	350	40	0.05	1/2	1/2	Y	Y	CH	0.13
15	350	40	0.05	1/2	1/2	Y	Y	Be	0.22
16	350	40	0.05	1/2	1/2	N	N	Al	4.6
17	350	40	0.05	1/2	1/2	Y	N	Al	0.73
18	200	40	0.02857	1/2	1/2	N	Y	Al	1.0
19	500	40	0.07143	1/2	1/2	N	Y	Al	4.9
20	200	40	0.02857	1/2	1/2	Y	Y	Al	0.10
21	500	40	0.07143	1/2	1/2	Y	Y	Al	0.091
22	350	40	0.05	1	1/2	N	Y	Al	8.1
23	350	40	0.05	2	1/2	N	Y	Al	9.8
24	350	40	0.05	1	1	N	Y	Al	1.7
25	350	40	0.05	1	1/2	Y	Y	Al	0.98
26	350	40	0.05	2	1/2	Y	Y	Al	4.6
27	350	40	0.05	1	1	Y	Y	Al	0.18
28	350	40	0.1	2	1/2	N	Y	Al	15.3
29	350	40	0.02	2	1/2	N	Y	Al	4.3
30	350	40	0.1	2	1/2	Y	Y	Al	2.0
31	350	40	0.02	2	1/2	Y	Y	Al	4.0
32	350	20	0.05	1/2	1/2	N	Y	Al	1.2
33	350	20	0.05	1/2	1/2	Y	Y	Al	6.5×10^{-4}

*N = No, Y = Yes

A final point is that some care has been exercised in insure that the MACH1 code treats both the electron and ion conductivity correctly in regions where there are large temperature gradients (Ref. 25).

3. RESULTS

Although the major result of the calculations, the neutron yield, is listed in Table 1, the results from two models are considered first in some detail. Model 6 is a case with the typical parameters described above and where the electron thermal conductivity is not suppressed. Figures 5 through 11 show the electron and ion temperatures, the energy flux due to electron thermal conduction and to radiation, the velocity, and the density plotted versus radius at various times for Model 6. Figure 5 shows these quantities at time $t = 0$ as discussed above (the initial conditions).

Figure 6 shows that the fuel-liner interface has moved to a radius of 0.36 cm. A strong shock is being driven into the fuel region. The energy dissipated in the shock is transferred to the ions, and the ion temperature is higher than the electron temperature just behind the shock. Electron thermal conduction is carrying energy ahead of the shock so the electron temperature is higher than the ion temperature near a radius of 0.30 cm. Note that a single strong shock brings the ion temperature in the fuel region to only 0.6 keV--not enough to achieve good burn. The density in the fuel region is low. The density in the liner shows a sharp spike near the interface. The energy flux plot shows how energy is loss from the fuel region. Electron thermal conduction transports energy from the fuel to the edge of the liner where it is radiated away. The fuel region itself is not dense enough to radiate effectively, but the liner is. It might be expected that either shutting off the thermal conduction or reducing the ability of the liner to radiate would decrease the loss of energy in the fuel and thereby increase the neutron yield.

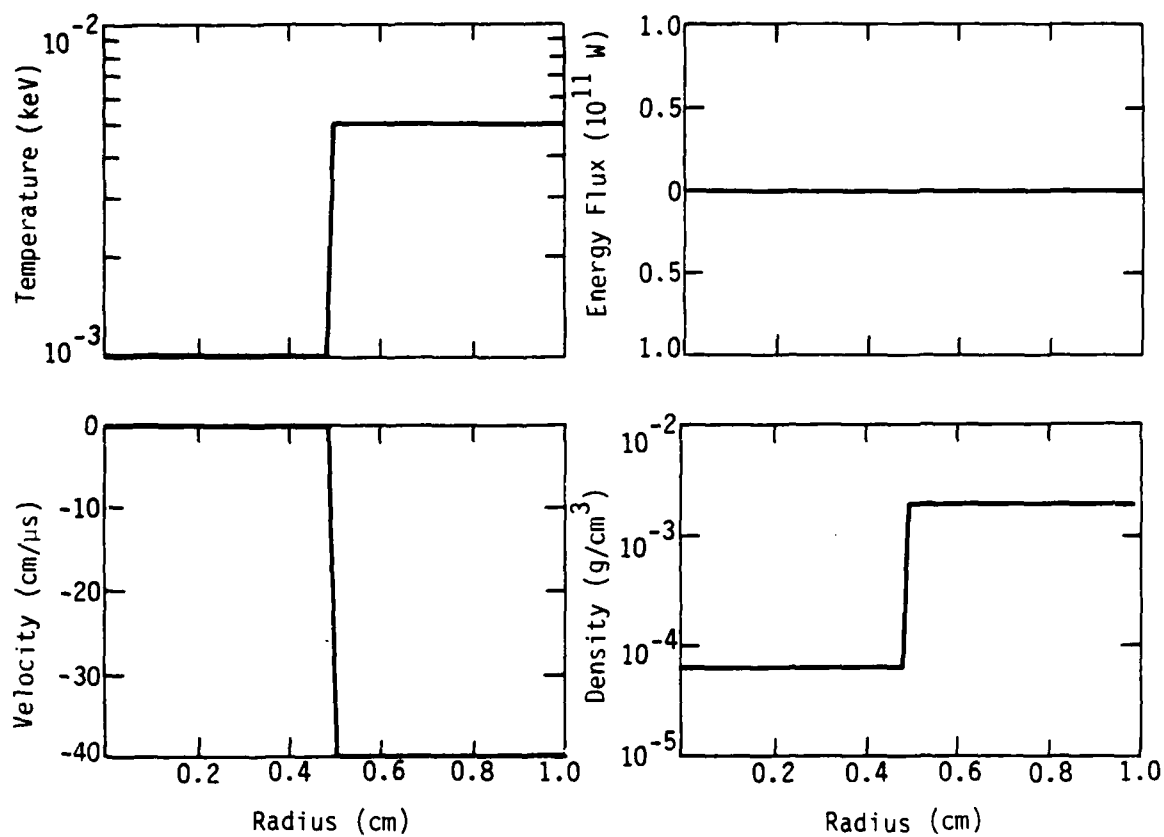


Figure 5. Temperature, energy flux, velocity, and density at time $t = 0$ for Models 6 and 2.

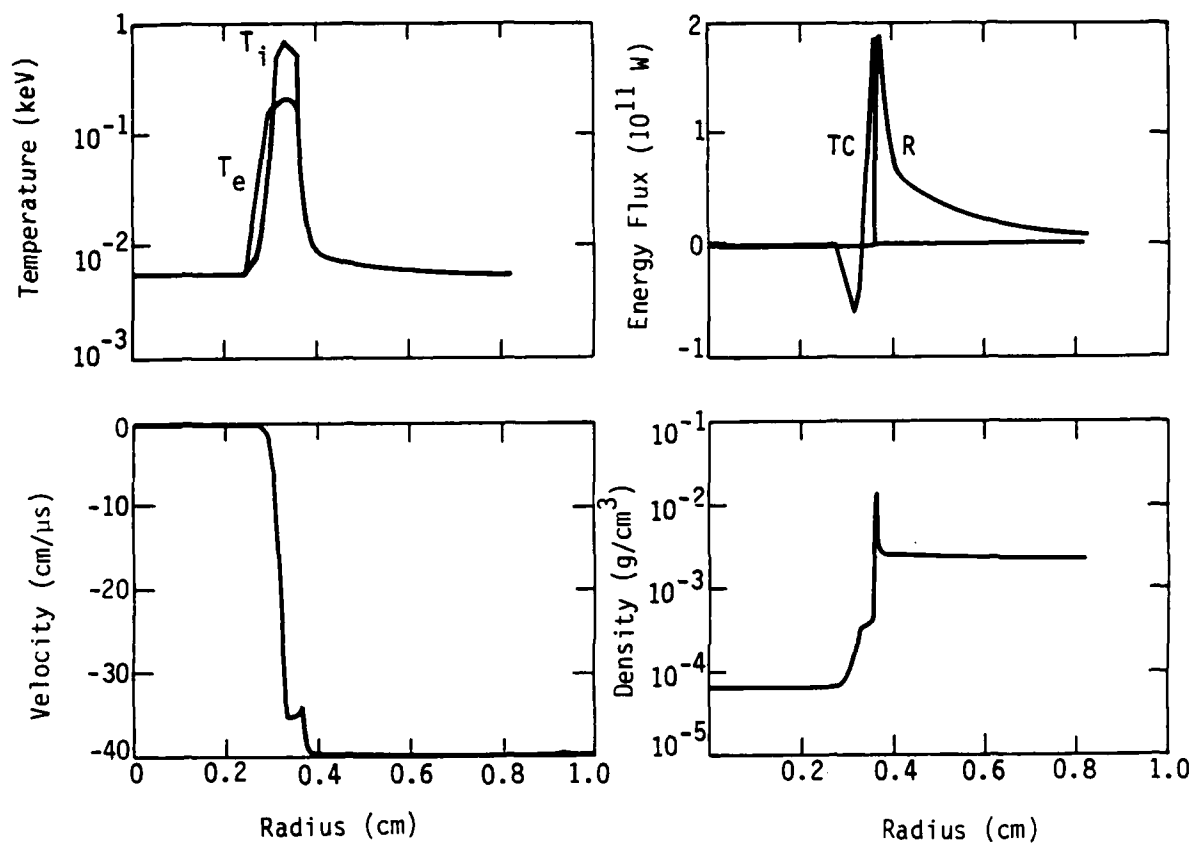


Figure 6. Temperature, energy flux velocity, and density at time $t = 4$ ns for Model 6. T_i is ion temperature. T_e is electron temperature. TC is electron thermal flux. R is radiation flux.

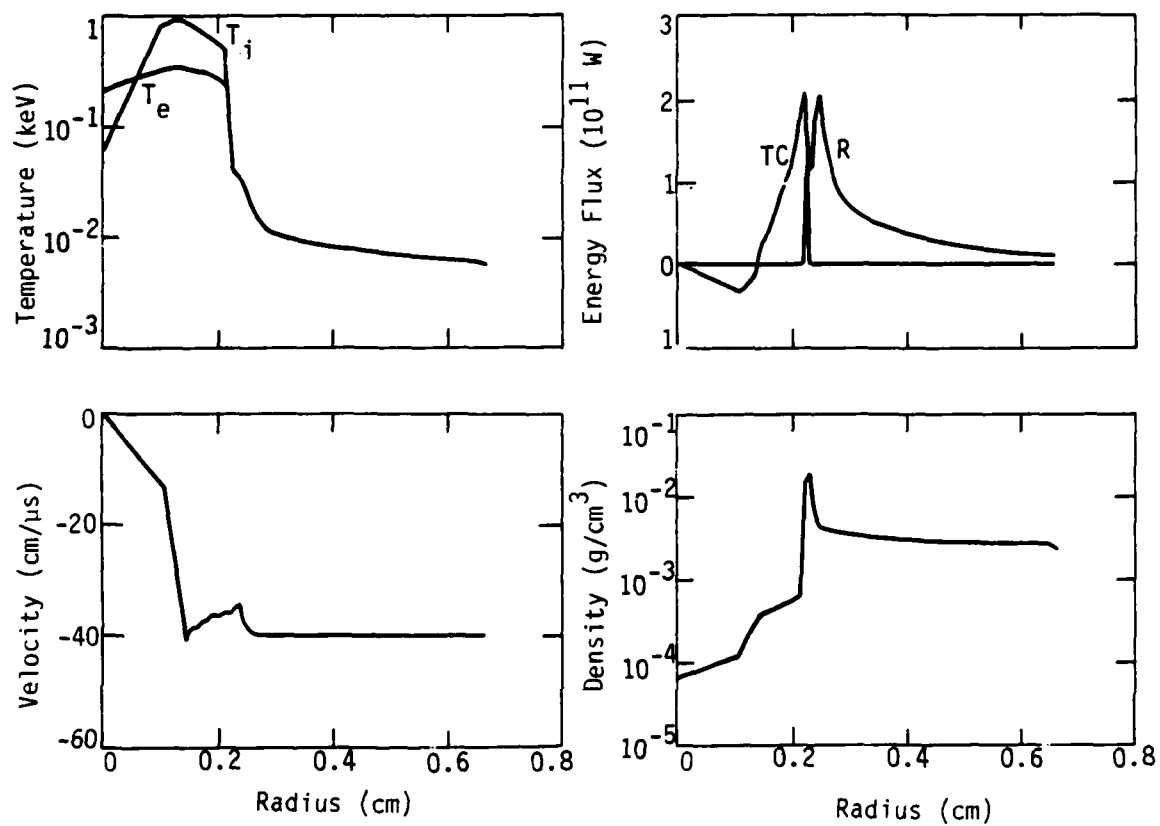


Figure 7. Temperature, energy flux, velocity, and density at time $t = 8$ ns for Model 6.

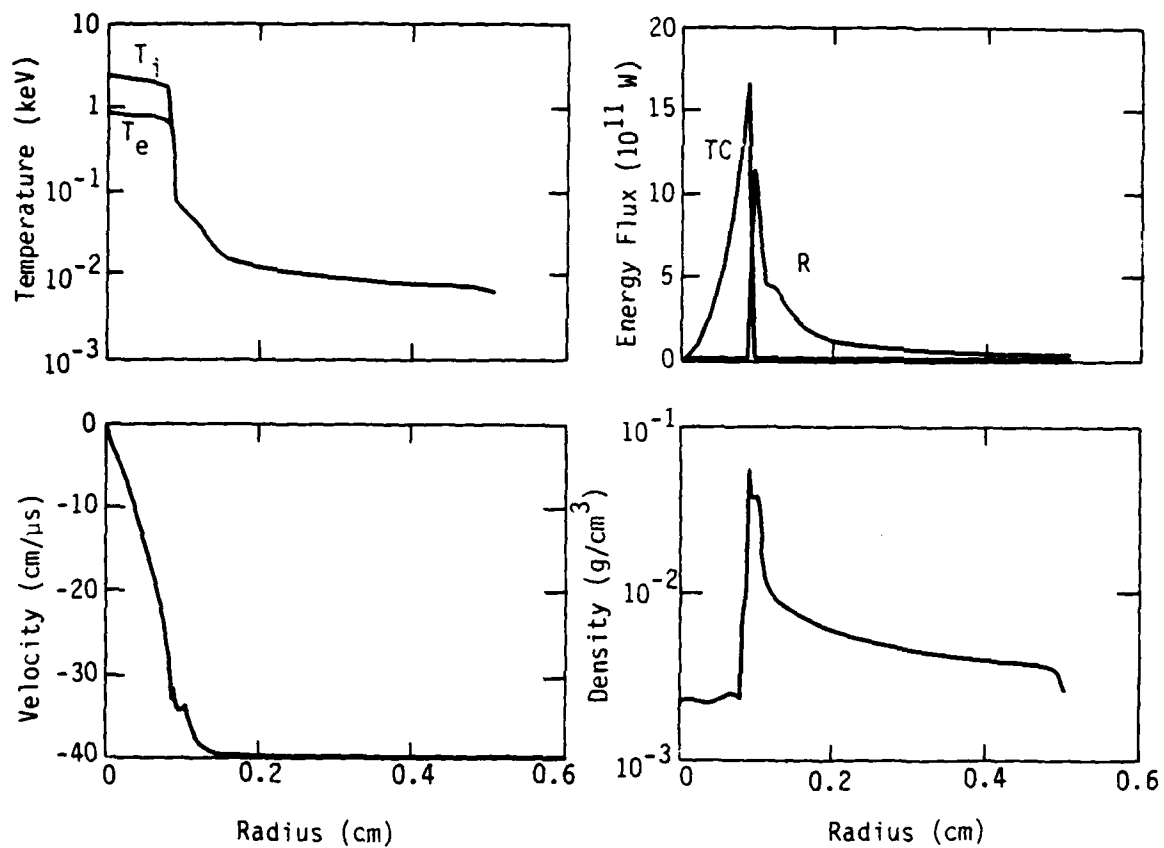


Figure 8. Temperature, energy flux, velocity, and density at time $t = 12$ ns for Model 6.

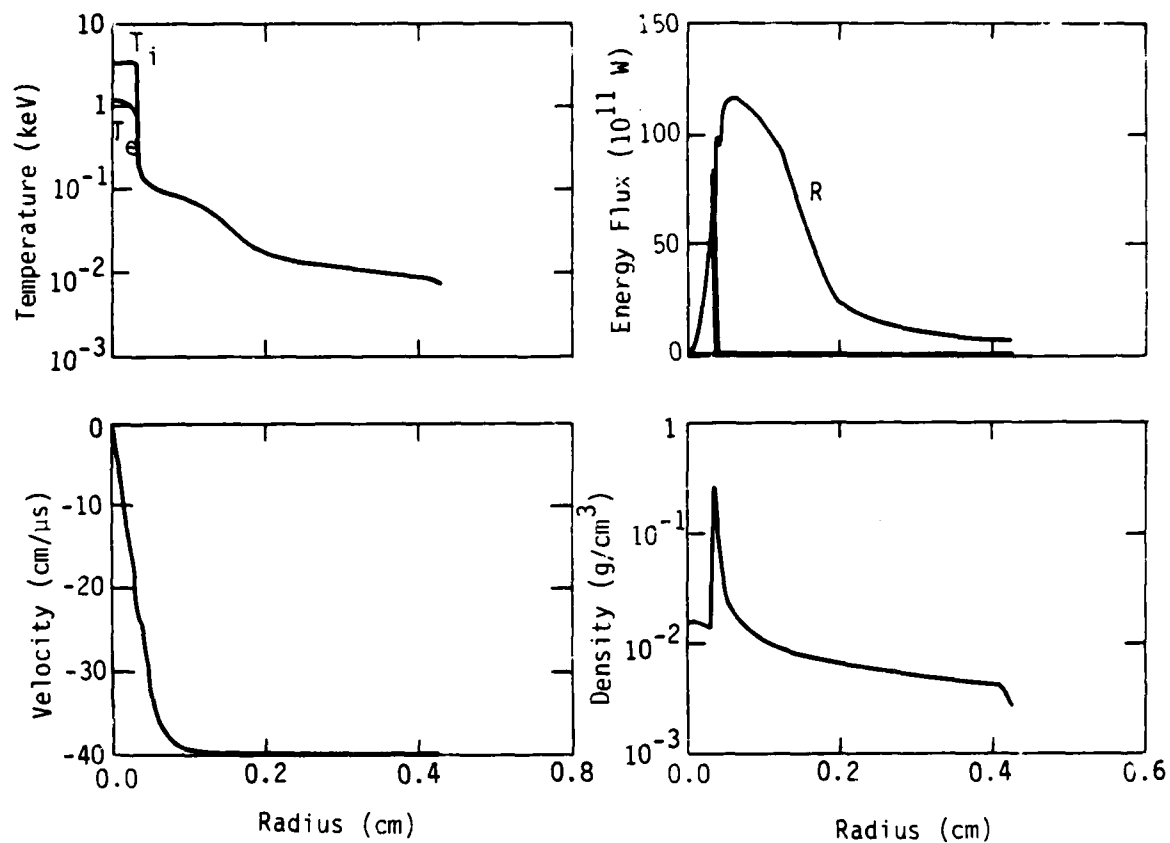


Figure 9. Temperature, energy flux, velocity, and density at time $t = 14$ ns for Model 6.

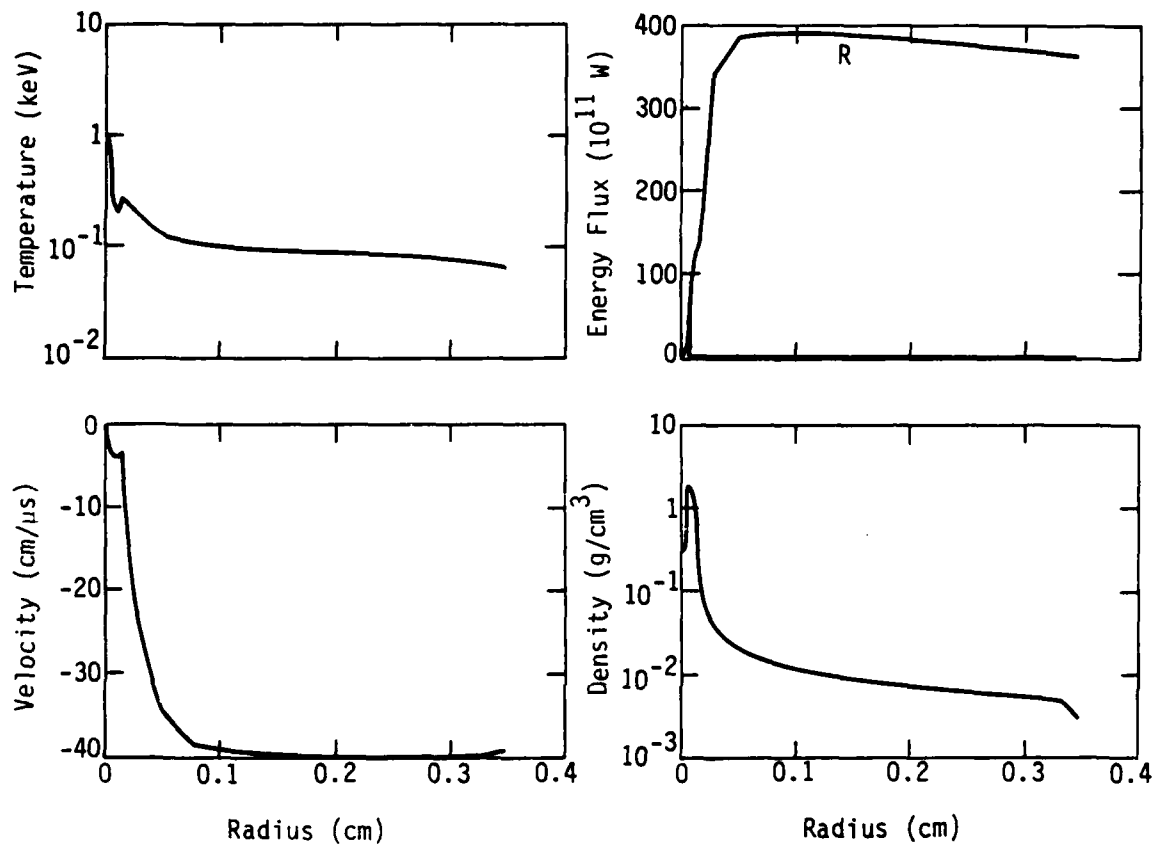


Figure 10. Temperature, energy flux, velocity, and density at time $t = 16$ ns for Model 6.

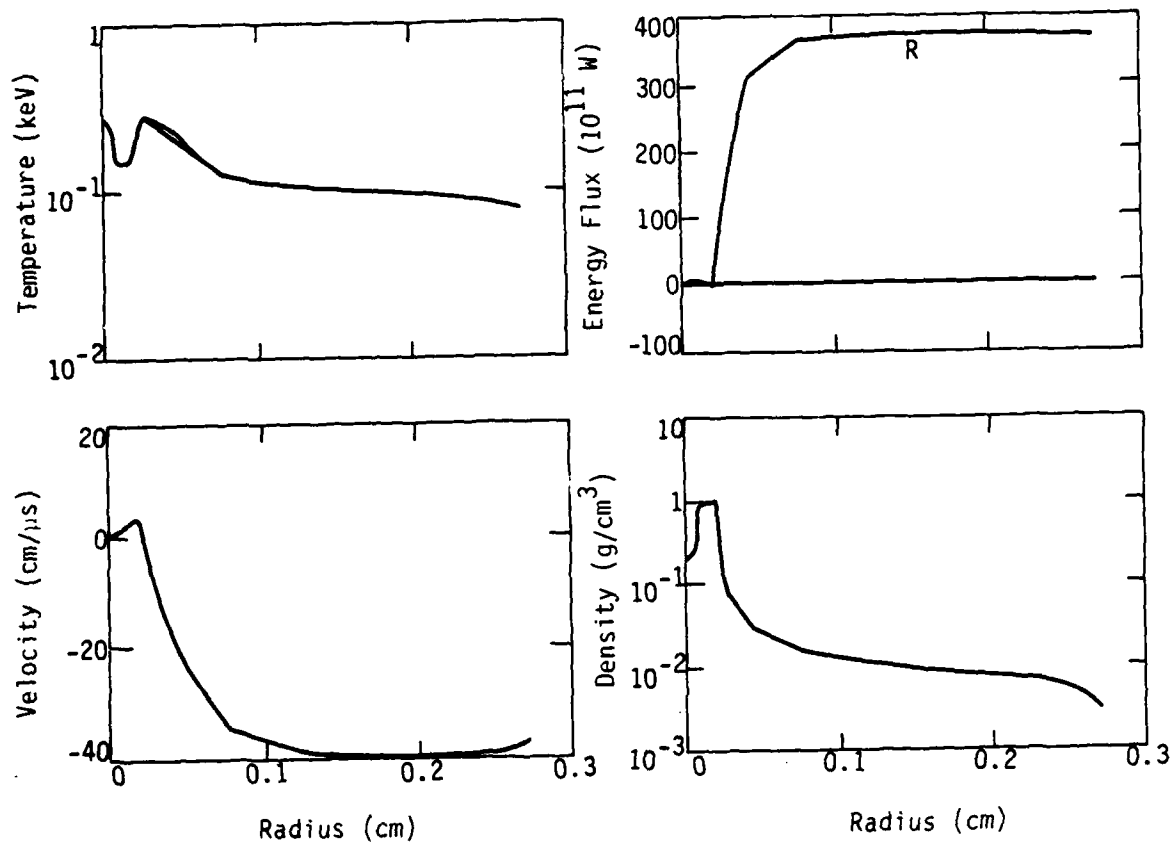


Figure 11. Temperature, energy flux, velocity, and density at time $t = 18$ ns for Model 6.

Figure 7 shows that the interface is at 0.22 cm at $t = 8$ ns. The first strong shock has almost reached the center.

At $t = 12$ ns, the interface is at 0.08 cm. The ion temperature in the fuel is 2 keV. The fuel density has increased by a factor 30 over the initial value. The thermal conduction is very large reaching a peak value of 1.7×10^{12} W.

At $t = 14$ ns, the interface is at 0.03 cm. The ion temperature is in excess of 3 keV. Energy losses due to electron thermal conduction are enormous. This is the time of maximum thermonuclear burn.

At $t = 16$ ns, the ion temperature has fallen to 1 keV. Energy is rapidly being transported from the center. Since the temperature cannot be maintained in the fuel region, there is not enough pressure to keep the liner from compressing the fuel to high density.

At $t = 18$ ns, the fuel temperature has dropped to less than 0.3 keV, and the thermonuclear burn is essentially over, while the plasma liner is still collapsing on axis.

Figure 12 shows the ion temperature, the density, the pressure, and the velocity of zones 1 (the central zone), 10 (half way through the fuel region by mass), 20 (outer edge of fuel), 21 (inner edge of plasma liner), 30 (a point in the interior of the liner) as a function of time. The peak in the ion temperature occurs before the peak in the density. The thermonuclear yield rate and the energies as a function of time are also shown in Figure 12. The yield rate has a sharp rise and an even sharper fall. Most of the original kinetic energy is ultimately converted to radiation. After a time of 10 ns, there is approximate pressure equilibrium in the fuel and the inner region of the liner. In Section IV, a pressure equilibrium was assumed between the fuel and tamper. The pressure curves illustrate the

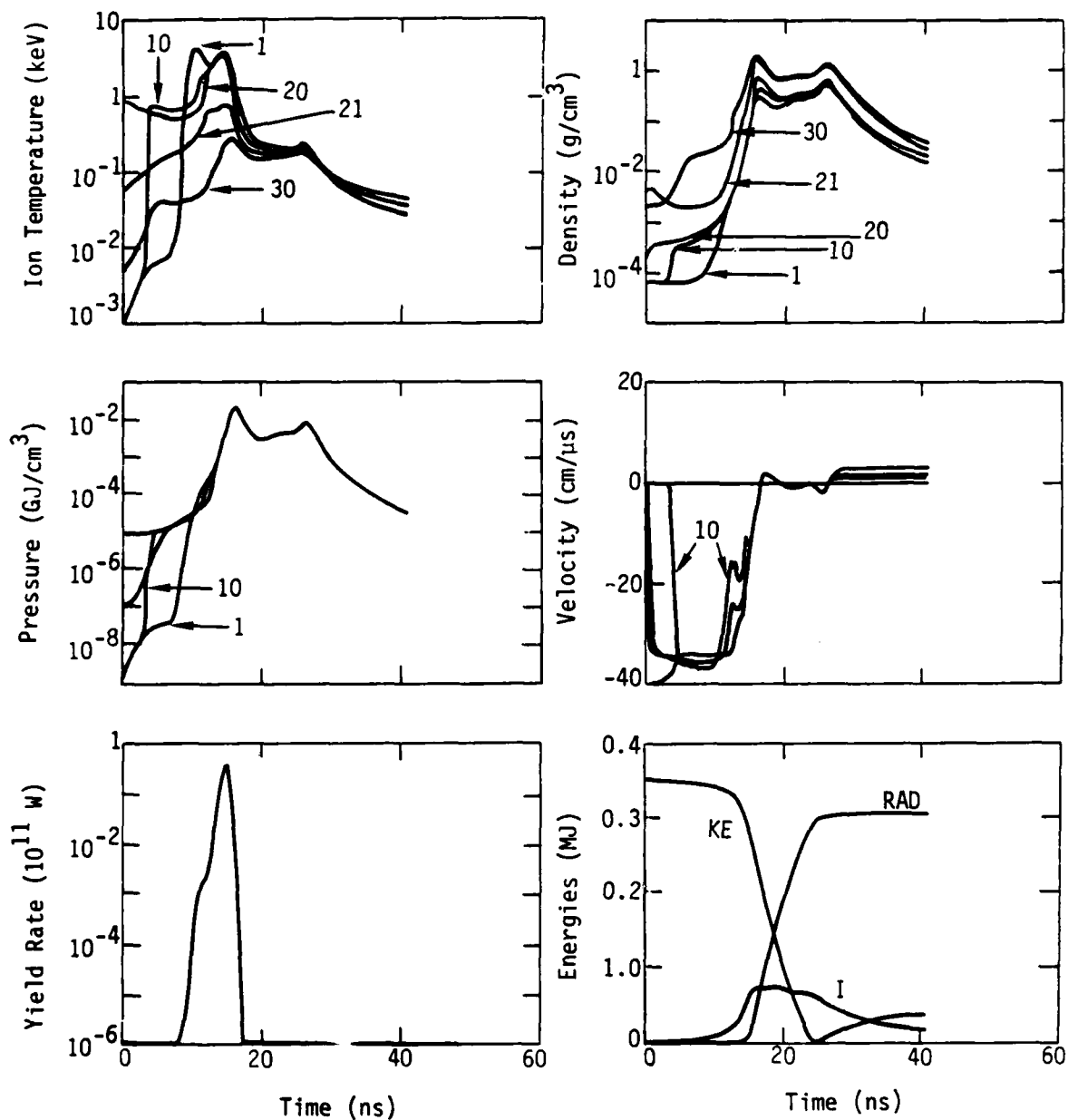


Figure 12. Ion temperature, density, pressure, velocity yield rate, and energy histories for Model 6. In the upper four plots, the quantities are for zones 1 (central zone), 10 (half way through the DT fuel region by mass), 20 (outer edge of fuel region), 21 (inner edge of liner), and 30 (in the liner, initially at radius 5.3 cm). In the energy plot, KE is the kinetic energy, I the internal energy, and RAD is the energy radiated away.

reasonableness of this assumption. There is some evidence for multiple shocks in the velocity plot for zone 10.

Model 2 is identical to Model 6 except that the electron thermal conduction is totally suppressed. Figure 5 is a plot of the initial conditions for Model 2 as well as for Model 6. Figures 13 through 18 for Model 2 should be compared to Figures 6-10 for Model 6.

Figure 13 is very similar to Figure 6 at time 4 ns. The temperatures in the shocked region are higher in Model 2 since the electron thermal conduction is suppressed. The radiation flux is slightly less in Model 2.

Figures 14 and 15 for Model 2 should be compared to Figures 6 and 8 for Model 6. The curves are again similar. The temperatures are higher and the radiation flux is lower in Model 2.

However, when Figure 16 is compared to Figure 10 there is a large difference. The fuel region in model 2 remains hot--there is no electron thermal conductivity to cool it. Since it is not cooled, the fuel pressure remains high, and the fuel density stays comparatively low. The minimum interface radius is 0.035 cm, which is a fuel compression of a factor 200. This is the time of maximum thermonuclear burn.

Figures 17 and 18 show that the fuel region remains hot even as it starts to expand. The ion temperature is still 4 keV at time 28 ns.

Figure 19 shows histories for Model 2 which should be compared to the histories for Model 6 shown in Figure 12. The fuel ion temperature is higher and the curve is broader for Model 2. The fuel density reaches a lower peak in Model 2. The velocity curve for zone 10 clearly shows the multiple shocks have been driven through the fuel. The maximum internal energy is higher in Model 2.

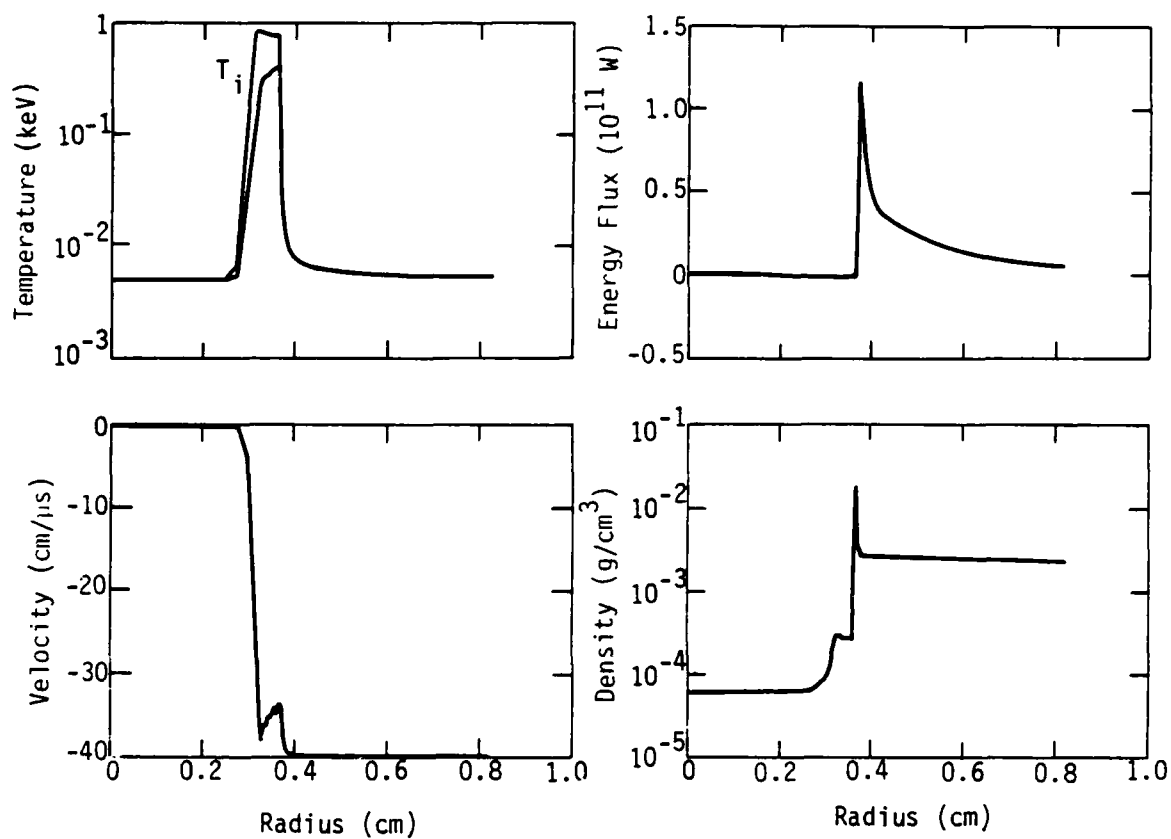


Figure 13. Temperature, energy flux, velocity, and density at time $t = 4$ ns for Model 2.

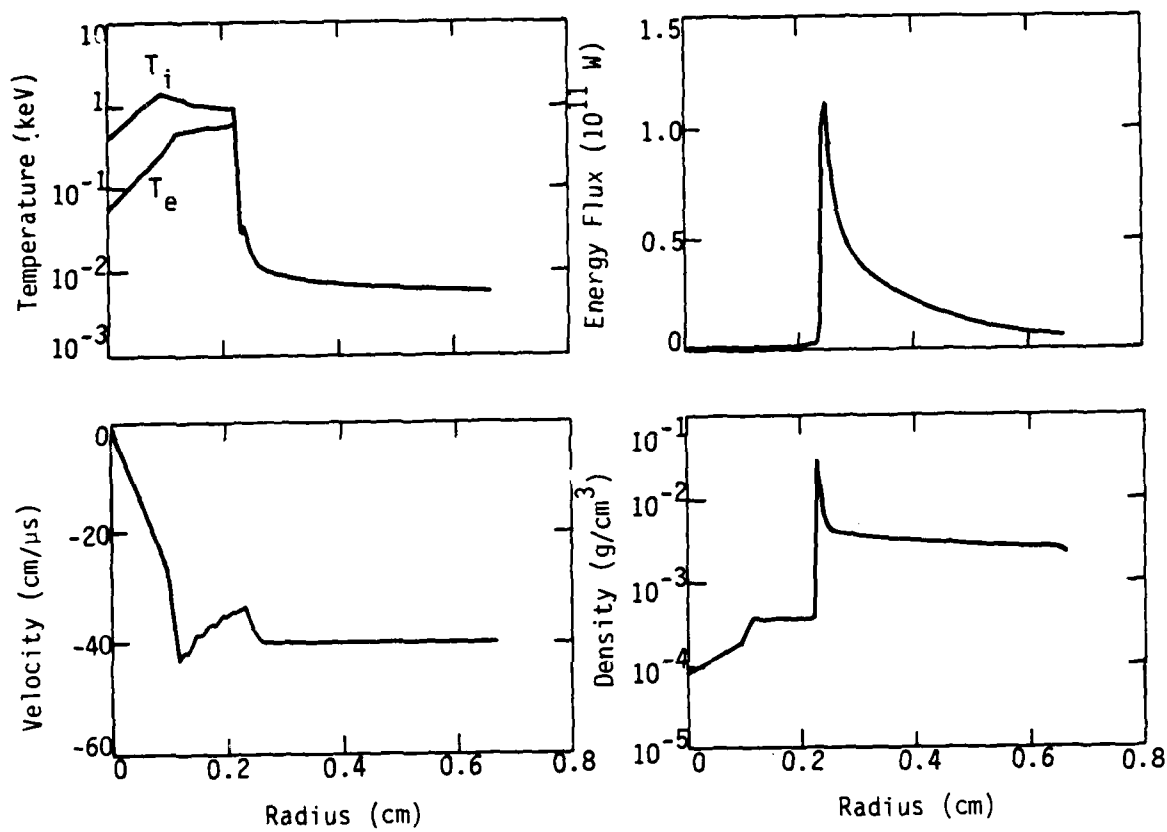


Figure 14. Temperature, energy flux, velocity, and density at time $t = 8$ ns for Model 2.

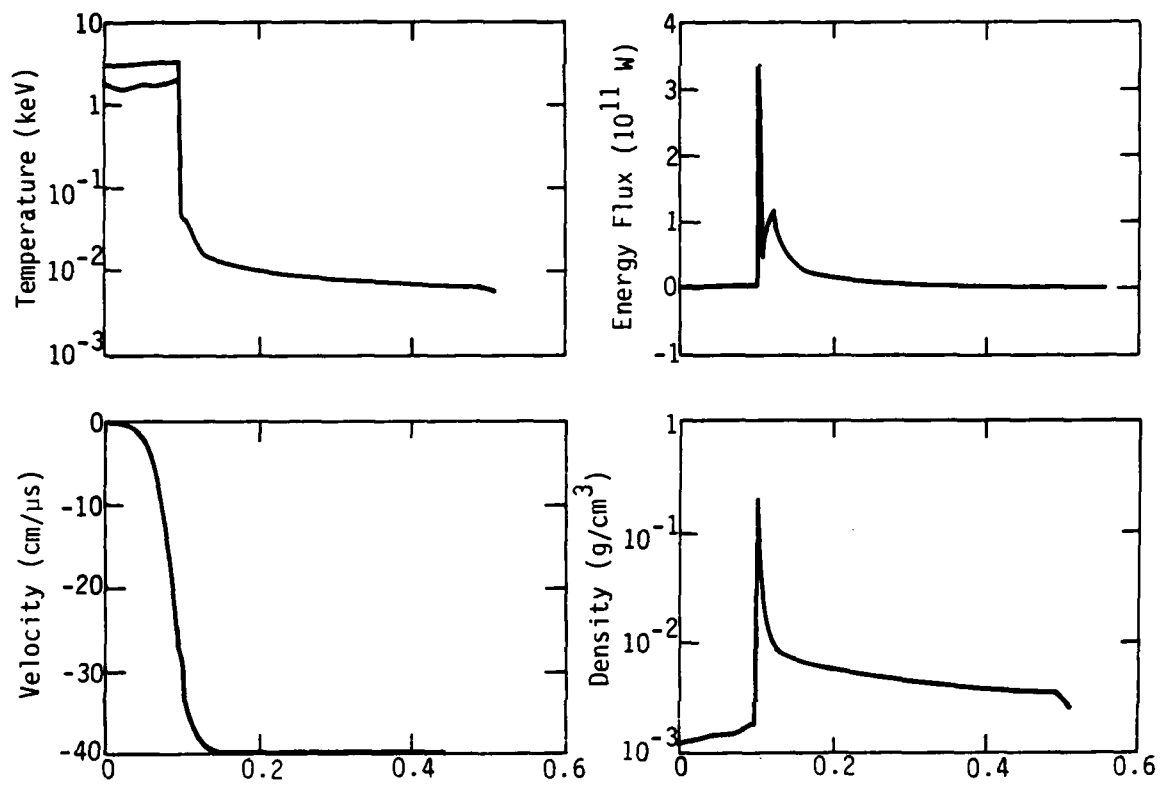


Figure 15. Temperature, energy flux, velocity, and density at time = 12 ns for Model 2.

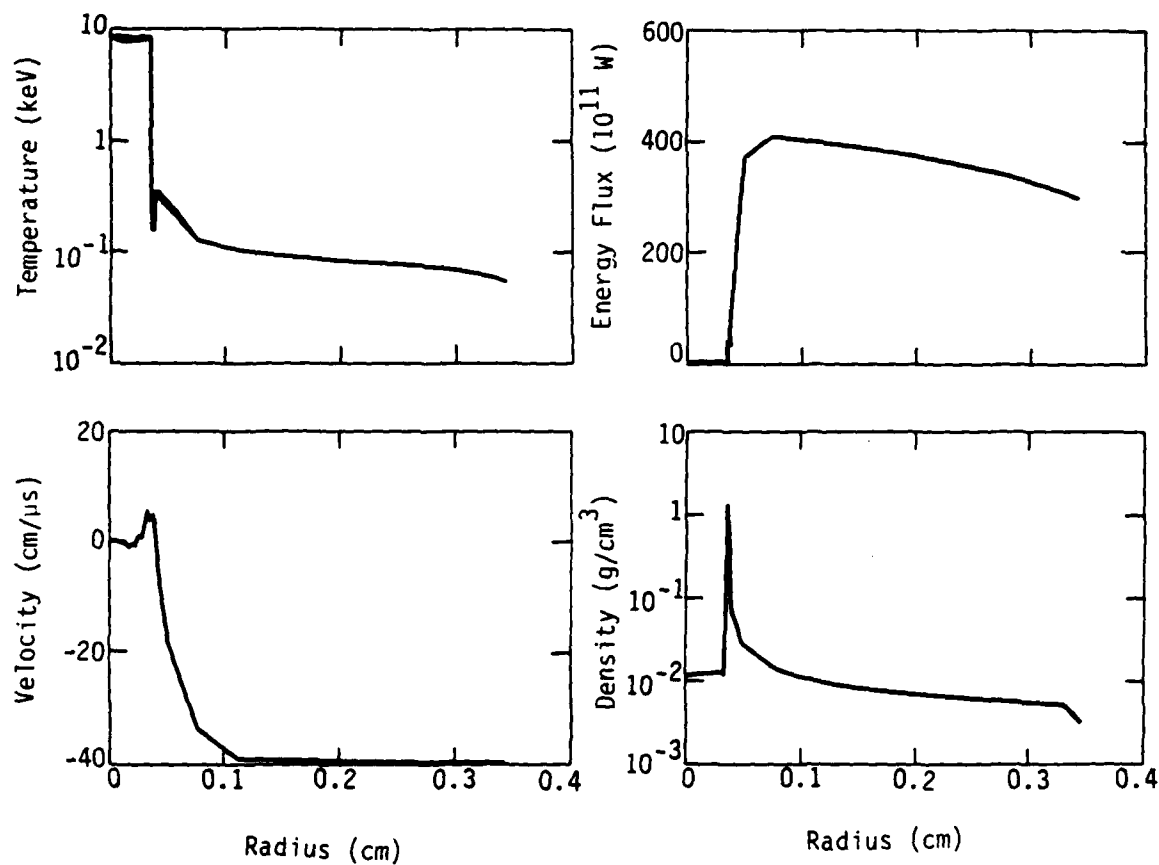


Figure 16. Temperature, energy flux, velocity, and density at time $t = 16$ ns for Model 2.

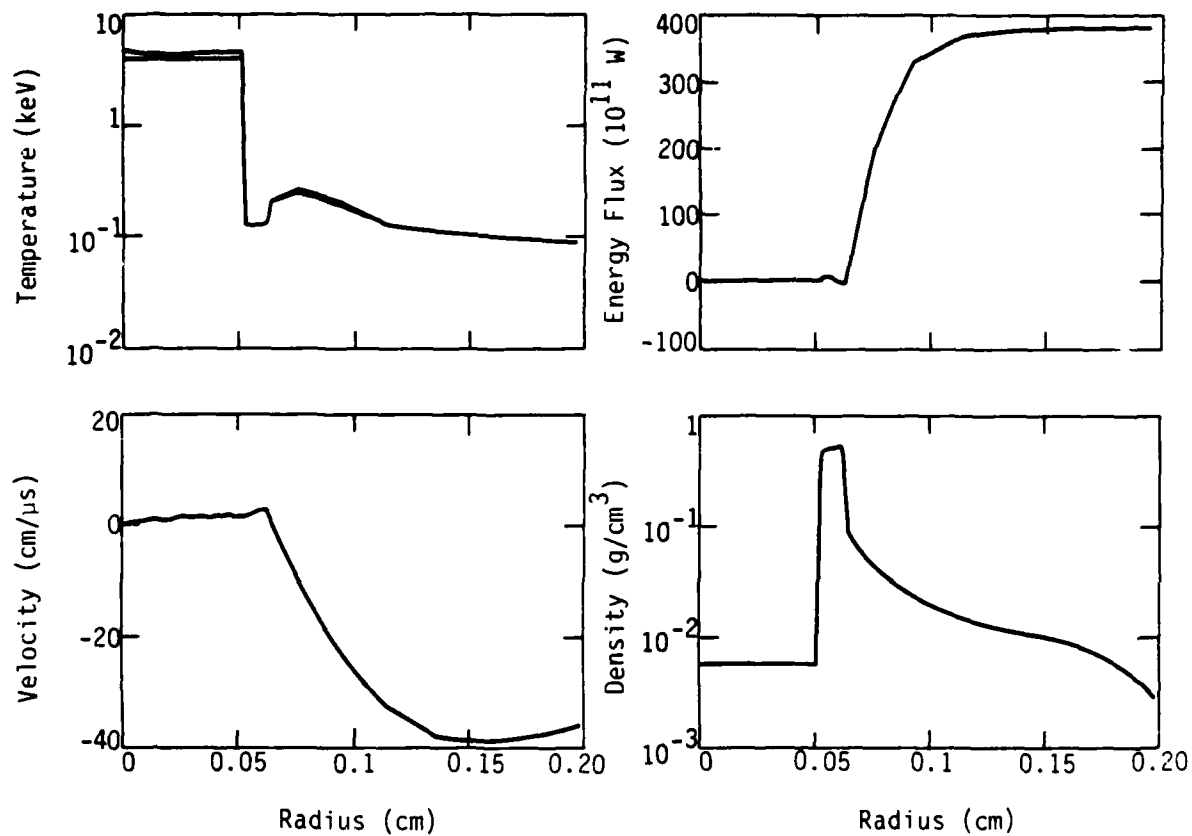


Figure 17. Temperature, energy flux, velocity, and density at time $t = 20$ ns for Model 2.

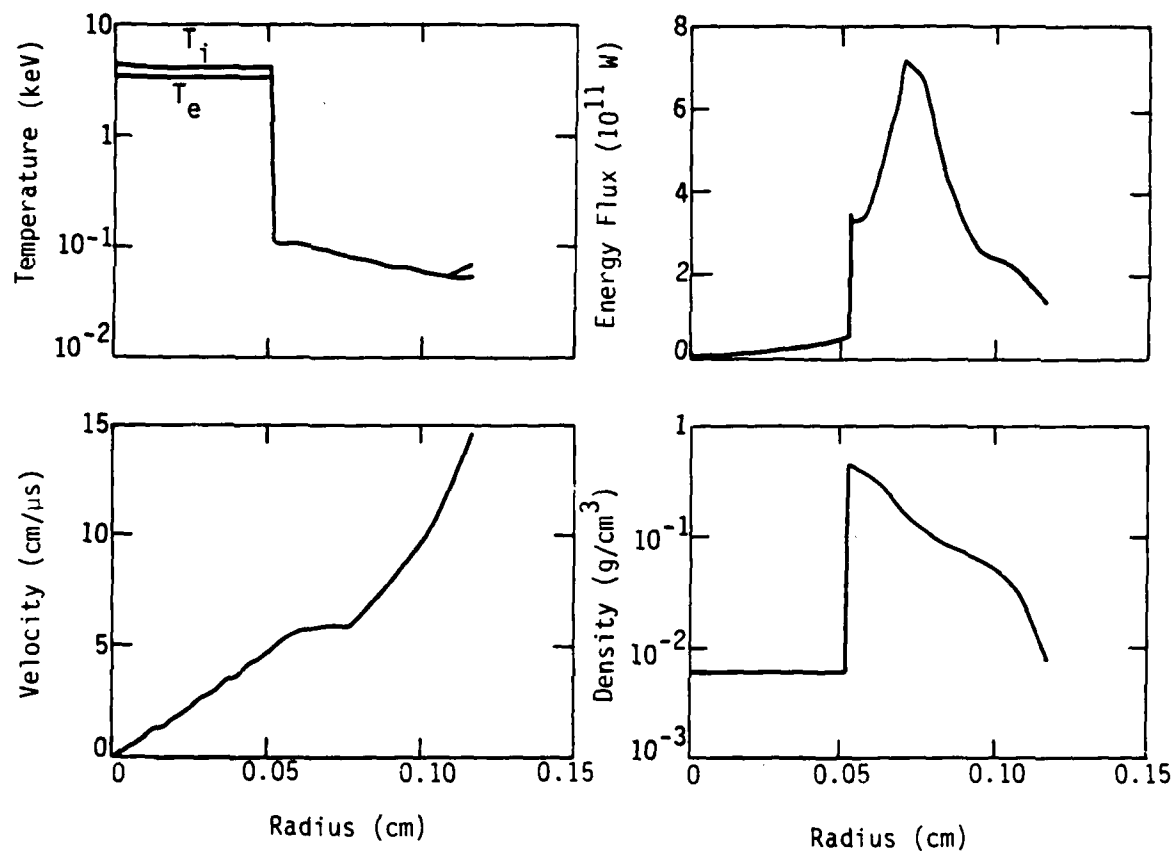


Figure 18. Temperature, energy flux, velocity, and density at time $t = 28$ ns for Model 2.

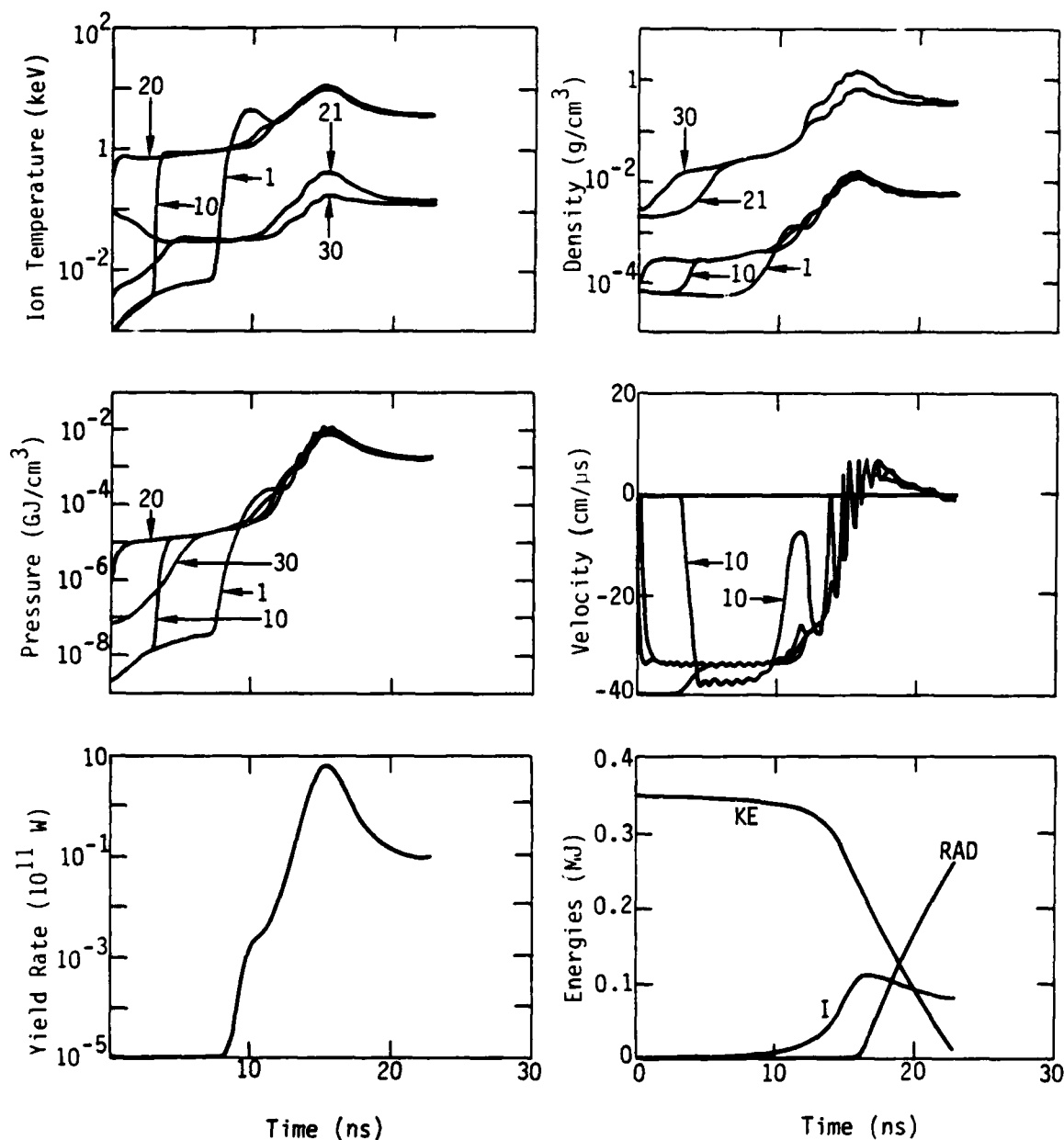


Figure 19. Ion temperature, density, pressure, velocity, yield rate, and energy histories for Model 2. In the upper four plots, the quantities are for zones 1 (central zone), 10 (half way through the DT fuel region by mass), 20 (outer edge of fuel region), 21 (inner edge of liner), and 30 (in the liner, initially at radius 5.3 cm). In the energy plot, KE is the kinetic energy, I the internal energy, and RAD is the energy radiated away.

The effects of variation of the input parameters are now considered. The last column of Table 1 gives the neutron production for the 33 models reported on here.

In Models 1 through 9, the fuel mass was varied. Models 1 through 4, in which the electron thermal conduction is suppressed, show little variation in neutron yield. The maximum production of 2.6×10^{15} n/cm is reached for a fuel mass of 0.05 mg (Model 2). Models 5 through 9, in which the conduction is not suppressed, show a large variation in neutron yield. The maximum production of 1.1×10^{15} n/cm is reached for a fuel mass of 0.01 mg. Lower fuel masses are required if the conduction cannot be suppressed by magnetic fields.

Models 2, 6, and 10 through 15 show the effects of different liner materials. When the conduction is suppressed, the variation in neutron production is small although high Z liners give somewhat better yields. If the conduction cannot be suppressed then, lower Z liners give better yields. This is easily understood, since the region in the liner near the fuel-liner interface cannot radiate as effectively in low Z materials. In Models 16 and 17 the radiation is turned off. These models are of no practical interest since there is no way to turn the radiation off in an experiment.

Models 2, 6, and 18 through 21 give the neutron production when the liner kinetic energy is changed. When the conduction is suppressed, the yield is strongly dependent on the input energy, varying from 1.0×10^{15} to 4.9×10^{15} n/cm as the kinetic energy is varied from 200 to 500 kJ/cm. There is very little variation in production when the electron conduction is not suppressed.

Models 2, 6, and 22 through 27 give the neutron production when the thickness of the liner and the thickness of the fuel region are varied.

Clearly, thicker fuel regions give much higher neutron yields. A thicker liner results in poorer performance. The fuel mass in Models 28 through 31 is varied as well as the thickness. Model 28 had the highest neutron production (1.5×10^{16} n/cm) of any model.

Models 32 and 33 show what happens when the liner velocity is lowered to 20 cm/ μ s. When conduction is suppressed, the yield is a factor 2.2 lower than in Model 2. When conduction is not suppressed, the yield is a factor 140 lower than in Model 6.

In conclusion, one would like to chose thick (>2 cm radius) DT fuel regions and one would like to keep the plasma liner as thin as possible. Fuel masses of about 0.1 mg are best if one believes that the electron conduction can be suppressed (as is most probably the case). The liner is about 2 cm long in the SHIVA STAR system. So the results from Model 28 would give a neutron yield of 3×10^{16} n for this sytem. When electron thermal conduction is supressed, there is suprisingly little variation in the neutron yield as the input parameters are varied. Indeed, most models in Table 1 with supressed conduction, could be roughly characterized as giving a neutron yield of a few $\times 10^{15}$ /cm. This lack of variation in yield gives one considerable confidence that an experiment on the SHIVA STAR system would be successful.

VII. FINAL COMMENTS

It has been shown that it will be extremely difficult to achieve good thermonuclear burn (>10 percent) in cylindrical targets driven by fast plasma liners with realistic parameters. Tamped cylindrical target systems require high compression ($\rho_f R_f \sim 0.1 \text{ g/cm}^2$) to achieve good burn. Given the symmetry in the current generation of imploding liner devices, this compression is extremely unlikely to be achieved in the near future. For low compression, wall confined targets with magnetothermoinsulation, other methods may be better choices.

A large neutron flux ($10^{15} - 3 \times 10^{16}$) can be produced in a simple fast liner-target system appropriate for the SHIVA STAR experiment. The neutron yield was not very sensitive to the input parameters as long as the electron thermal conductivity was suppressed at the liner fuel interface. The neutron production was highest when the fuel radius was large ($>2 \text{ cm}$). Hussey (Ref. 26) has suggested that a low density gas fill may help to stabilize the plasma liner during the run in phase of the implosion. If the fill gas is DT, then the neutrons produced could be a powerful diagnostic in determining the quality of the plasma implosion. In the future, it would be desirable to have one-dimensional and two-dimensional magneto-hydrodynamic calculations of this concept.

REFERENCES

1. Mokhov, V. N., V. K. Chernyshev, V. B. Yakubov, M. S. Protasov, V. M. Danov, and E. I. Zharinov, "Controlled Thermonuclear Fusion Based on Magnetogasdynamic Energy Storage," Soviet Physics - Doklady, 24, p. 557, 1979.
2. Alikhanov, S. G. and V. P. Bakhtin, Investigation of the M=0 Instability of a θ -Pinch Liner for Three-Dimensional Plasma Compression, IAE preprint, 3543/8, 1982.
3. Toepfer, A. J., Hydrodynamically Coupled Pellets, P11R-8-80, Physics International Company, San Leandro, CA, 1980.
4. Linhart, J. G., "Very-High-Density Plasmas for Thermonuclear Fusion," Nucl. Fusion, 10, p. 211, 1970.
5. Linhart, J. G. "Rocket-Driven Liners for Fusion Triggers and for Very-High-Density Reactors," Nucl. Fusion, 13, p. 321, 1973.
6. Varnum, W. S., "Electrically Imploded Cylindrical Fusion Targets," Nucl. Fusion, 15, p. 1183, 1975.
7. Somon, J. P. and C. Jablon, "Efficiency of Fluid Compression by a Supersonic Heavy Liner," Nucl. Fusion, 16, p. 1040, 1976.
8. Shearer, J. W. and W. C. Condit, "Magnetically Driven Metal Liners for Plasma Compression," Energy Storage, Compression, and Switching, (Bostick, W. H., Nardi, V., Zucher, O. S. F. Eds), Plenum Publishing Corp., New York, NY, 1976.
9. Jablon, C. and C. Rioux, "Thermonuclear Energy Production of a Cylindrical Plasma Imploded by a Heavy Liner," Nucl. Fusion, 16, p. 791, 1976.
10. Sherwood, A. R., B. L. Freeman, R. A. Gerwin, T. R. Jarboe, R. A. Krakowski, R. C. Malone, J. Marshall, R. L. Miller, B. Saydam, R. L. Hagenson, E. L. Kemp, R. W. Moses and C. E. Swannack, Fast Liner Proposal, LA-6707-P, Los Alamos National Laboratory, Los Alamos, NM, August 1977.
11. Lindemuth, I. R. and T. R. Jarboe, "Initial Numerical Studies of the Behavior of Z-Pinch Plasma Under Liner Implosion Conditions," Nucl. Fusion, 28, p. 929, 1978.
12. Gerwin, R. A. and R. C. Malone, "A Adiabatic Plasma Heating and Fusion-Energy Production by a Compressible Fast Liner," Nucl. Fusion, 19, p. 155, 1979.

REFERENCES (Continued)

13. Reinovsky, R. E., D. L. Smith, W. L. Baker, J. H. Degnan, R. P. Henderson, B. J. Kohn, D. A. Kloc, and N. F. Roderick, IEEE Trans. on Plasma Sci., "Inductive Store Pulse Compression System for Driving High Speed Plasma Implosions," PS-10, p. 73, 1982.
14. Mason, R. J. and R. L. Morse, "Tamped Thermonuclear Burn of DT-Microspheres," Nucl. Fusion, 15, p. 935, 1975.
15. Lindemuth, I. R. and R. C. Kirkpatrick, Parameter Space for Magnetized Fuel Targets in Inertial Confinement Fusion, LA-UR-82-1900, Los Alamos National Laboratory, Los Alamos, NM, 1982.
16. Spitzer, L., Physics of Fully Ionized Gases, 2nd Ed., Interscience, New York, NY, 1962.
17. Braginskii, S. I., "Transport Processes in a Plasma," Reviews of Modern Physics, (Leontovich, M. A. Ed.), Vol. 1, Consultants Bureau, New York, NY, p. 205, 1965.
18. Lindemuth, I. R. and M. M. Widner, "Magnetohydrodynamic Behavior of Thermonuclear Fuel in a Preconditioned Electron Beam Imploded Target," Phys. Fluids, 24 p. 746, 1981.
19. Alme, M. L. and J. R. Wilson, "X Ray Emission From a Neutron Star Accreting Material," The Astrophysical Journal, 186, p. 1015, 1973.
20. Glenn, D., A Users Guide for MACH1, AMRC-R-357, Mission Research Corporation, Albuquerque, NM, September 1981.
21. Kmetyk, L. N., "Thermonuclear Burn in Wall-Confined Plasmas," Phys. Fluids, 24, p. 970, 1981.
22. Kmetyk, L. N. and R. A. Gross, "Energy Gains of a Wall-Confined Fusion Cycle," Phys. Fluids, 25, p. 1042, 1982.
23. Degnan, J. H. and R. E. Reinovsky, On Forming Cylindrical Gas Shells in Electrode Gaps for Electromagnetic Implosion Plasma Generation, AFWL-TR-75-265, Air Force Weapons Laboratory, Kirtland Air Force Base, NM, 1976.
24. Degnan, J. H., R. E. Reinovsky, D. L. Honea, and R. D. Bengston, "Electromagnetic Implosions of Cylindrical Gas 'Shells'," J. Appl. Phys. 52, p. 6550, 1981.
25. Frese, M. H., Steady State Based Boundary Averaging Scheme for Power Law Thermal Flux Coefficients, AMRC-N-144, Mission Research Corporation, Albuquerque, NM, 1980.

REFERENCES (Concluded)

26. Hussey, T. W., "Snowplow Stabilization of the Hydromagnetic Raleigh-Taylor Instability in Imploded Foil Plasmas," Bull. American Phys. Society, 27, p. 1065, 1982.